NASA TECHNICAL MEMORANDUM

NASA TM X-1345

NASA TM X-1345

STATIC AERODYNAMIC CHARACTERISTICS OF A MODEL OF A TYPICAL SUBSONIC JET-TRANSPORT AIRPLANE AT MACH NUMBERS FROM 0.40 TO 1.20

by Eugene N. Brooks, Jr., John P. Decker, and James A. Blackwell, Jr.

Langley Research Center
Langley Station, Hampton, Va.

NATIONAL AERONAUTICS AND SPACE ADMINISTRATION • WASHINGTON, D. C. • FEBRUARY 1967

NASA TM X-1345

STATIC AERODYNAMIC CHARACTERISTICS OF A MODEL OF A TYPICAL SUBSONIC JET-TRANSPORT AIRPLANE AT MACH NUMBERS FROM 0.40 TO 1.20

By Eugene N. Brooks, Jr., John P. Decker,
and James A. Blackwell, Jr.

Langley Research Center
Langley Station, Hampton, Va.

NATIONAL AERONAUTICS AND SPACE ADMINISTRATION

For sale by the Clearinghouse for Federal Scientific and Technical Information
Springfield, Virginia 22151 – Price $2.00

STATIC AERODYNAMIC CHARACTERISTICS OF A MODEL OF A TYPICAL SUBSONIC JET-TRANSPORT AIRPLANE AT MACH NUMBERS FROM 0.40 TO 1.20

By Eugene N. Brooks, Jr., John P. Decker,
and James A. Blackwell, Jr.
Langley Research Center

SUMMARY

An investigation was conducted in the Langley 8-foot transonic pressure tunnel to determine the static aerodynamic characteristics of a model of a typical subsonic, swept-wing, jet-transport airplane at large angles of attack and transonic Mach numbers. The Mach number range extended from 0.40 to 1.20 and the angle-of-attack range from -8° to 18°.

The results indicate that the model was longitudinally stable at zero sideslip angle for lift coefficients between 0.15 to 0.50 corresponding to angles of attack up to about 3° throughout the Mach number range. In the same lift-coefficient range and at Mach numbers above 0.90, the model exhibited large increases in static margin with small changes in Mach number. At lift coefficients between 0.50 and 0.80, the static margin decreased to approximately zero for Mach numbers between 0.40 and 0.80. At lift coefficients greater than 0.80, corresponding to angles of attack greater than 7°, the model was longitudinally stable at all Mach numbers except between 0.95 and 1.03.

For small sideslip angles and at Mach numbers below 0.90, the model had positive effective dihedral; however, the model had negative effective dihedral for Mach numbers of 0.90 and 0.95 over significant portions of the lift-coefficient range. At a Mach number of 0.90, the model was longitudinally unstable for a sideslip angle of 5° in about the same lift-coefficient range in which the effective dihedral was negative. Weathercock stability was maintained for all Mach numbers and angles of attack.

INTRODUCTION

The National Aeronautics and Space Administration is studying the aerodynamic characteristics and handling qualities of large swept-wing, subsonic, jet-transport aircraft to aid in determining the piloting procedures necessary to recover from high angle-of-attack and transonic Mach number conditions sometimes encountered in very turbulent

air. It is known that transport airplanes similar to the configuration of this study have encountered turbulent conditions in flight and have dived rapidly and reached Mach numbers as high as 1.08. Theoretical predictions of the static and dynamic aerodynamic characteristics of subsonic jet-transport-airplane configurations are available, but these predictions are not considered applicable at high angles of attack and transonic Mach numbers. To provide accurate dynamic data at the angles of attack and Mach numbers of interest in this study, the dynamic characteristics of a model of a typical subsonic jet-transport airplane have been investigated and reported in reference 1.

As a continuation of the dynamic stability study and as part of the overall program, the purpose of the present investigation is to provide the static aerodynamic stability data for the model of reference 1. Tests were conducted in the Langley 8-foot transonic pressure tunnel over a Mach number range of 0.40 to 1.20, an angle-of-attack range from about -8° to 18°, and generally at angles of sideslip of 0°, 2°, and 5°.

SYMBOLS

The results are presented as force and moment coefficients with the longitudinal aerodynamic parameters referred to the stability system of axes and the lateral aerodynamic parameters referred to the body system of axes. The origin for these axes systems is the moment reference center of the model which is located at the quarter chord of the mean aerodynamic chord of the wing. (See fig. 1.) Measurements are given in the International System of Units (SI) and parenthetically in the U.S. Customary Units. Conversion factors for these units are given in reference 2. The symbols are defined as follows:

b	wing span, 0.997 meter (3.271 ft)
$\bar{c}$	mean aerodynamic chord of wing, 0.154 meter (0.504 ft)
M	free-stream Mach number
q	free-stream dynamic pressure, newtons/meter^2 (lbf/ft^2)
R	Reynolds number based on $\bar{c}$
r	radius
S	reference wing area, 0.148 meter^2 (1.597 ft^2)

α angle of attack referred to body reference axis, deg

β angle of sideslip, deg

C_L lift coefficient, $\frac{\text{Lift}}{qS}$

C_m pitching-moment coefficient, $\frac{\text{Pitching moment}}{qS\bar{c}}$

C_l rolling-moment coefficient, $\frac{\text{Rolling moment}}{qSb}$

C_n yawing-moment coefficient, $\frac{\text{Yawing moment}}{qSb}$

C_Y side-force coefficient, $\frac{\text{Side force}}{qS}$

C_{L_α} lift-curve slope $\frac{\partial C_L}{\partial \alpha}$ measured from $C_L = 0.15$ to $C_L = 0.50$

$C_{m_{C_L}}$ static margin $\frac{\partial C_m}{\partial C_L}$ measured from $C_L = 0.15$ to $C_L = 0.50$

C_{l_β} effective dihedral parameter, $\frac{\Delta C_l}{\Delta \beta}$, $\Delta\beta \approx 2^\circ$

C_{n_β} directional-stability parameter, $\frac{\Delta C_n}{\Delta \beta}$, $\Delta\beta \approx 2^\circ$

C_{Y_β} side-force parameter, $\frac{\Delta C_Y}{\Delta \beta}$, $\Delta\beta \approx 2^\circ$

DESCRIPTION OF THE MODEL

The physical characteristics and dimensions of the test model, which are considered representative of current subsonic jet-transport-airplane configurations, are presented in figure 1. Photographs showing two views of the model are shown in figure 2. Table I presents several geometric properties of the wing, horizontal tail, and vertical tail and table II presents airfoil coordinates for the same components.

The model had a low swept wing with four jet-engine nacelles mounted beneath the wing on slab pylons. The portion of the wing inboard of the innermost pylons had a leading-edge sweepback angle of 41.5° and outboard of these inner pylons, a leading-edge sweepback angle of 37.5°. The horizontal tail was set at an incidence angle of 0°. In order to retain the actual fuselage afterbody closure, the sting was designed to enter the model at the bottom of the fuselage at an angle of 6° with respect to the body reference axis. The model geometry and configuration were fixed throughout the test, and there were no movable control surfaces.

TESTS, APPARATUS, AND CORRECTIONS

The investigation was conducted in the Langley 8-foot transonic pressure tunnel, which is a rectangular, single-return wind tunnel with slotted test section. Tests were conducted for a Mach number range from 0.40 to 1.20, an angle-of-attack range from about -8° to 18°, and generally at angles of sideslip of approximately 0°, 2°, and 5°. The variation of the test Reynolds number, based on the mean aerodynamic chord, with Mach number is as shown in figure 3 unless noted otherwise.

Tests were conducted with boundary-layer transition fixed with 0.25-centimeter-wide (0.10-in.-wide) strips of No. 80 carborundum grains set in a plastic adhesive. The three-dimensional roughness was applied with the forward edges of the strips positioned (1) 0.76 cm (0.30 in.) behind the leading edge of the wing and engine nacelles (2) 0.864 cm (0.34 in.) rearward from the tip of the nose (3) 0.508 cm (0.20 in.) rearward from the leading edge of the horizontal tail and (4) 0.66 cm (0.26 in.) rearward from the leading edge of the vertical tail. (All distances were measured in the streamwise direction.)

Force and moment measurements were made with a six-component internally mounted strain-gage balance. The angles of attack and sideslip were corrected for deflection of the balance and sting under aerodynamic loads and for tunnel flow angularity. Corrections were not made for sting interference effects caused by the sting entering the fuselage from beneath the model rather than from the rear of the model. The sting interference could affect the longitudinal and the lateral-directional aerodynamic characteristics. The accuracy of the data based upon repeatability and static calibrations is as follows:

C_L	±0.01
C_m	±0.005
C_l	±0.0005
C_n	±0.0005
C_Y	±0.005
α, degree	±0.1
β, degree	±0.1
M	±0.003

PRESENTATION OF RESULTS

The results of this investigation have been reduced to coefficient and parameter form. The basic longitudinal aerodynamic data are presented in figure 4 and summarized in figure 5. The basic lateral aerodynamic data are presented in figures 6 and 7 and summarized in figures 8 and 9. To aid in the location of data, the following list is given:

DISCUSSION

Longitudinal Aerodynamic Characteristics

Figure 4 shows the curves for the variation of angle of attack with lift coefficient to be essentially linear between $C_L = 0.15$ and $C_L = 0.50$ throughout the Mach number range. At lift coefficients above about 0.50 and at Mach numbers up to 0.925, the curves became nonlinear and the lift-curve slopes decreased to less than one-half the values measured in the C_L range from 0.15 to 0.50. At Mach numbers above 0.925, similar results are shown; however, decreases in lift-curve slope were delayed to lift coefficients of approximately 0.80. The lift-curve slope, as measured between $C_L = 0.15$ and 0.50, is shown in figure 5 to have increased with Mach number up to 0.80. At Mach numbers above 0.80, C_{L_α} decreases, and a lift-curve slope "bucket" is shown at a Mach number of 0.925; this condition is typical of high-aspect-ratio thick wings.

In figure 4 the pitching-moment curves are shown to be essentially linear and the model remains stable between $C_L = 0.15$ and 0.50 for all Mach numbers. At lift coefficients between 0.50 and 0.80 (that is, between $\alpha = 3^\circ$ and 7°), the static margin decreased to approximately zero for Mach numbers between 0.40 and 0.80. At lift coefficients greater than 0.80 (that is, α above approximately 7°), the model was

longitudinally stable at all Mach numbers except at Mach numbers between 0.95 and 1.03 where some longitudinal instability is indicated. At the Mach numbers at which negative lift coefficients were investigated, the model is longitudinally stable except at $M = 0.95$ where longitudinal instability is indicated in the C_L range from -0.25 to -0.05.

The static margin $C_{m_{C_L}}$ (fig.5) remains practically invariant for Mach numbers from 0.40 to 0.90. At Mach numbers above 0.90, large increases in static margin with small changes in Mach number are indicated. These increases in static margin amount to a rearward shift in the aerodynamic center of $0.34\bar{c}$ with only a 0.15 increase in Mach number.

Lateral Aerodynamic Characteristics

Figure 6 shows the rolling-moment coefficient C_l, yawing-moment coefficient C_n, and side-force coefficient C_Y to be essentially linear between $\beta = \pm 2^\circ$. Both the effective dihedral and the weathercock stability decreased at large sideslip angles (that is, above approximately 7°) at all Mach numbers and angles of attack except at $M = 0.90$ and $\alpha = 3.20^\circ$, where the effective dihedral was negative $\left(+C_{l_\beta}\right)$ at small sideslip angles but positive $\left(-C_{l_\beta}\right)$ at large sideslip angles; and at $M = 0.95$ and $\alpha = 3.15^\circ$, where the positive effective dihedral increased with increasing sideslip angle.

Since C_l, C_n, and C_Y were only linear between $\beta = \pm 2^\circ$ for all Mach numbers, the lateral-directional stability parameters shown in figures 8 and 9 were computed by using the data of figure 7 and taking finite differences in the coefficients between $\beta = 0^\circ$ and 2°.

Figure 8 shows that at the lower Mach numbers the model had positive effective dihedral $\left(-C_{l_\beta}\right)$ throughout the lift-coefficient range. However, at $M = 0.90$ and 0.95, the model had negative effective dihedral $\left(+C_{l_\beta}\right)$ at the lower lift coefficients. Figure 7(d) shows that at approximately the same lift coefficients that negative effective dihedral was exhibited at $M = 0.90$, pitch nonlinearities existed for $\beta \approx 5.09^\circ$.

Figures 8 and 9 show that the weathercock stability was maintained and that the directional stability derivative C_{n_β} varied between 0.0016 and 0.0039 throughout the Mach number and lift-coefficient ranges. The side-force parameter C_{Y_β} is seen in figures 8 and 9 to be practically invariant with Mach number and lift coefficient and deviates very little from a value of -0.02.

SUMMARY OF RESULTS

Results of an aerodynamic investigation of a model of a typical swept-wing subsonic jet-transport airplane conducted over an angle-of-attack range from about -8° to 18°, at

Mach numbers from 0.40 to to 1.20, and generally at angles of sideslip of 0°, 2°, and 5°, indicate the following:

1. Between lift coefficients of 0.15 and 0.50 the lift curves were essentially linear for all Mach numbers, but for lift coefficients above 0.50 and at Mach numbers up to 0.925 the lift curves became nonlinear and the lift-curve slopes decreased to less than one-half the value measured between lift coefficients of 0.15 and 0.50.

2. At zero sideslip angle the model was longitudinally stable over a lift-coefficient range from 0.15 to 0.50 for all Mach numbers. The static margin for this lift range remained practically invariant up to a Mach number of 0.90. At Mach numbers above 0.90 the model exhibited large increases in static margin with small changes in Mach number. At lift coefficients between 0.50 and 0.80 the static margin decreased to approximately zero for Mach numbers between 0.40 and 0.80. Longitudinal instabilities are indicated for lift coefficients above 0.80 at Mach numbers between 0.95 and 1.03 and for negative lift coefficients at a Mach number of 0.95.

3. At Mach numbers below 0.90 the model had positive effective dihedral for small sideslip angles. However, at Mach numbers of 0.90 and 0.95 negative effective dihedral was exhibited over significant portions of the lift-coefficient range. At a Mach number of 0.90 the model also developed pitch nonlinearities at a sideslip angle of approximately 5° in about the same lift-coefficient range in which the effective dihedral was negative.

4. For small sideslip angles weathercock stability was maintained throughout the Mach number and angle-of-attack ranges of this investigation.

Langley Research Center,
National Aeronautics and Space Administration,
Langley Station, Hampton, Va., October 26, 1966,
126-13-01-31-23.

REFERENCES

1. Wright, Bruce R.; and Brower, Margaret L: Aerodynamic Damping and Oscillatory Stability in Pitch for a Model of a Typical Subsonic Jet-Transport Airplane. NASA TN D-3159, 1966.

2. Mechtly, E. A.: The International System of Units – Physical Constants and Conversion Factors. NASA SP-7012, 1964.

TABLE I.- GEOMETRIC PROPERTIES OF WING, HORIZONTAL TAIL, AND VERTICAL TAIL

Wing:	
Area,	
meters^2	0.1413
ft^2	1.5209
Span,	
meters	0.9970
ft	3.2710
Mean aerodynamic chord,	
meters	0.1536
ft	0.5039
Aspect ratio	7.035
Taper ratio	0.33
Geometric dihedral, deg	7
Horizontal tail:	
Area,	
meters^2	0.0321
ft^2	0.3455
Span,	
meters	0.3304
ft	1.0840
Mean aerodynamic chord,	
meters	0.1015
ft	0.3330
Root chord,	
meters	0.1359
ft	0.4459
Aspect ratio	3.43
Taper ratio	0.41
Geometric dihedral, deg	7
Vertical tail:	
Area,	
meters^2	0.0196
ft^2	0.2110
Mean aerodynamic chord,	
meters	0.1125
ft	0.3691
Aspect ratio	1.80
Taper ratio	0.31

TABLE II.- AIRFOIL COORDINATES

[Stations and ordinates have been nondimensionalized with respect to airfoil chord]

(a) Wing

Upper surface		Lower surface		Upper surface		Lower surface		Upper surface		Lower surface	
Station	Ordinate	Station	Ordinate	Station	Ordinate	Station	Ordinate	Station	Ordinate	Station	Ordinate
0	0.0297	0	0.0297	0	0.0236	0	0.0236	0	0	0	0
.0050	.0442	.0050	.0152	.0050	.0357	.0050	.0146	.0050	.0149	.0050	-.0066
.0075	.0462	.0075	.0132	.0074	.0382	.0074	.0115	.0083	.0165	.0083	-.0074
.0125	.0502	.0125	.0096	.0126	.0421	.0126	.0089	.0125	.0206	.0125	-.0083
.0250	.0588	.0250	.0017	.0250	.0523	.0250	.0032	.0249	.0256	.0249	-.0091
.0499	.0667	.0499	-.0066	.0500	.0631	.0500	-.0051	.0500	.0330	.0500	-.0099
.0750	.0719	.0750	-.0132	.0750	.0676	.0750	-.0102	.0748	.0396	.0748	-.0124
.1000	.0743	.1000	-.0198	.1000	.0727	.1000	-.0159	.1000	.0446	.1000	-.0132
.1500	.0756	.1500	-.0303	.1500	.0778	.1500	-.0242	.1500	.0545	.1500	-.0165
.2000	.0743	.2000	-.0376	.2000	.0803	.2000	-.0319	.2000	.0578	.2000	-.0215
.2500	.0719	.2500	-.0429	.2500	.0790	.2500	-.0382	.2500	.0628	.2500	-.0248
.2075	.0680	.2075	-.0462	.3000	.0784	.3000	-.0433	.3000	.0661	.3000	-.0297
.4000	.0595	.4000	-.0456	.4000	.0752	.4000	-.0459	.4000	.0661	.4000	-.0297
.5000	.0502	.5000	-.0383	.5000	.0726	.5000	-.0459	.5000	.0611	.5000	-.0289
.6000	.0416	.6000	-.0311	.6000	.0561	.6000	-.0408	.6000	.0512	.6000	-.0264
.7000	.0330	.7000	-.0231	1.0000	0	1.0000	0	.7000	.0413	.7000	-.0198
.8000	.0251	.8000	-.0152					1.0000	0	1.0000	0
.8999	.0145	.8999	-.0080								
1.0000	0	1.0000	0								
Span station: 0.0403 meter (0.1323 ft) Chord length: 0.2747 meter (0.9012 ft)				Span station: 0.0953 meter (0.3125 ft) Chord length: 0.1993 meter (0.6538 ft)				Span station: 0.2000 meter (0.6562 ft) Chord length: 0.1537 meter (0.5042 ft)			

Upper surface		Lower surface		Upper surface		Lower surface	
Station	Ordinate	Station	Ordinate	Station	Ordinate	Station	Ordinate
0	0.0030	0	0	0	0.0032	0	0
.0050	.0099	.0050	-.0046	.0050	.0100	.0050	-.0046
.0074	.0120	.0074	-.0055	.0075	.0121	.0075	-.0057
.0126	.0147	.0126	-.0065	.0125	.0161	.0125	-.0064
.0250	.0215	.0250	-.0074	.0250	.0214	.0250	-.0075
.0500	.0303	.0500	-.0090	.0500	.0314	.0500	-.0089
.0753	.0385	.0753	-.0105	.0750	.0386	.0750	-.0104
.1000	.0442	.1000	-.0118	.1000	.0443	.1000	-.0118
.1500	.0520	.1500	-.0149	.1500	.0521	.1500	-.0146
.2000	.0570	.2000	-.0177	.2000	.0571	.2000	-.0179
.2500	.0604	.2500	-.0206	.2500	.0604	.2500	-.0204
.3000	.0627	.3000	-.0227	.3000	.0629	.3000	-.0229
.4000	.0644	.4000	-.0253	.4000	.0646	.4000	-.0254
.5000	.0618	.5000	-.0250	.4071	.0618	.4071	-.0250
.6000	.0541	.6000	-.0208	.6000	.0543	.6000	-.0207
.7000	.0427	.7000	-.0156	.7000	.0429	.7000	-.0157
.8000	.0290	.8000	-.0105	.8000	.0289	.8000	-.0104
.9000	.0145	.9000	-.0051	.9000	.0161	.9000	-.0054
1.0000	0	1.0000	0	1.0000	0	1.0000	0
Span station: 0.2688 meter (0.8819 ft) Chord length: 0.1333 meter (0.4372 ft)				Span station: 0.4953 meter (1.6250 ft) Chord length: 0.0711 meter (0.2333 ft)			

TABLE II.- AIRFOIL COORDINATES - Concluded

[Stations and ordinates have been nondimensionalized with respect to airfoil chord]

(b) Horizontal tail

Upper surface		Lower surface		Upper surface		Lower surface		Upper surface		Lower surface		Upper surface		Lower surface	
Station	Ordinate	Station	Ordinate	Station	Ordinate	Station	Ordinate	Station	Ordinate	Station	Ordinate	Station	Ordinate	Station	Ordinate
0	0.0142	0	0.0142	0	0.0131	0	0.0131	0	0.0124	0	0.0124	0	0.0127	0	0.0127
.0050	.0250	.0050	.0026	.0051	.0204	.0051	.0018	.0051	.0221	.0051	.0020	.0050	.0223	.0050	.0018
.0075	.0267	.0075	.0004	.0075	.0248	.0075	.0002	.0076	.0236	.0076	.0001	.0075	.0236	.0065	0
.0125	.0283	.0125	-.0026	.0124	.0268	.0124	-.0024	.0124	.0254	.0124	-.0025	.0125	.0254	.0125	-.0023
.0250	.0317	.0250	-.0078	.0251	.0295	.0251	-.0073	.0249	.0279	.0249	-.0051	.0250	.0282	.0250	-.0050
.0500	.0347	.0500	-.0151	.0499	.0319	.0499	-.0142	.0500	.0305	.0500	-.0135	.0500	.0304	.0500	-.0136
.0750	.0364	.0750	-.0207	.0750	.0337	.0750	-.0193	.0749	.0323	.0749	-.0185	.0750	.0323	.0750	-.0186
.1000	.0377	.1000	-.0258	.1000	.0348	.1000	-.0237	.1001	.0333	.1001	-.0226	.1000	.0332	.1000	-.0227
.1500	.0403	.1500	-.0338	.1500	.0373	.1500	-.0313	.1501	.0353	.1501	-.0295	.1500	.0355	.1500	-.0295
.2000	.0428	.2000	-.0398	.2001	.0393	.2001	-.0366	.1999	.0376	.1999	-.0348	.2000	.0377	.2000	-.0350
.2500	.0452	.2500	-.0444	.2500	.0417	.2500	-.0408	.2499	.0396	.2499	-.0389	.2500	.0395	.2500	-.0386
.3000	.0476	.3000	-.0476	.2999	.0437	.2999	-.0437	.3000	.0417	.3000	-.0417	.3000	.0418	.3000	-.0418
.3500	.0498	.3500	-.0498	.3500	.0459	.3500	-.0459	.3500	.0437	.3500	-.0437	.3500	.0436	.3500	-.0436
.4000	.0512	.4000	-.0511	.4000	.0472	.4000	-.0472	.4001	.0447	.4001	-.0447	.4000	.0445	.4000	-.0445
.5000	.0504	.5000	-.0504	.5000	.0466	.5000	-.0466	.5001	.0447	.5001	-.0447	.5000	.0445	.5000	-.0445
.6000	.0442	.6000	-.0442	.6000	.0424	.6000	-.0424	.5999	.0414	.5999	-.0414	.6000	.0414	.6000	-.0414
.7000	.0338	.7000	-.0338	.7001	.0337	.7001	-.0337	.7000	.0338	.7000	-.0338	.7000	.0336	.7000	-.0336
.8000	.0226	.8000	-.0226	.7999	.0224	.7999	-.0224	.8001	.0226	.8001	-.0226	.8000	.0227	.8000	-.0227
.9000	.0114	.9000	-.0114	.9000	.0118	.9000	-.0118	.9002	.0112	.9002	-.0112	.9000	.0114	.9000	-.0114
1.0000	0	1.0000	0	1.0000	0	1.0000	0	1.0000	0	1.000	0	1.0000	0	1.0000	0
Span station: 0 meter (0 ft) Chord length: 0.1359 meter (0.4459 ft)				Span station: 0.0434 meter (0.1423 ft) Chord length: 0.1145 meter (0.3757 ft)				Span station: 0.0726 meter (0.2381 ft) Chord length: 0.1000 meter (0.3281 ft)				Span station: 0.1652 meter (0.5420 ft) Chord length: 0.0559 meter (0.1834 ft)			

(c) Vertical tail

Station	Ordinate	Station	Ordinate	Station	Ordinate	Station	Ordinate
0	0	0	0	0	0	0	0
.0049	.0084	.0050	.0075	.0050	.0070	.0050	.0069
.0075	.0102	.0075	.0091	.0074	.0084	.0073	.0082
.0126	.0127	.0125	.0123	.0124	.0106	.0123	.0105
.0250	.0172	.0250	.0154	.0251	.0142	.0251	.0142
.0500	.0239	.0500	.0212	.0501	.0196	.0498	.0197
.0750	.0291	.0750	.0259	.0749	.0238	.0750	.0238
.0999	.0334	.1000	.0296	.1000	.0275	.1001	.0274
.1501	.0407	.1499	.0357	.1501	.0331	.1500	.0329
.2000	.0455	.2001	.0403	.2000	.0373	.1998	.0375
.2500	.0495	.2501	.0439	.2501	.0405	.2501	.0407
.3000	.0524	.3001	.0464	.3000	.0429	.3000	.0430
.3499	.0541	.3501	.0480	.3501	.0443	.3498	.0444
.4001	.0549	.4000	.0487	.4000	.0449	.4001	.0448
.5000	.0517	.5000	.0469	.5000	.0443	.5002	.0444
.5999	.0434	.6000	.0414	.6000	.0407	.5999	.0407
.7000	.0318	.7001	.0328	.7000	.0339	.7000	.0329
.8000	.0221	.8001	.0228	.8000	.0236	.8002	.0238
.8838	.0116	.9000	.0129	.9000	.0144	.8999	.0142
1.0000	.0016	1.0000	.0019	1.0000	.0020	1.0000	.0046
Span station: 0 meter (0 ft) Chord length: 0.1596 meter (0.5237 ft) Leading-edge radius: 0.0013 meter (0.0044 ft)		Span station: 0.0301 meter (0.0988 ft) Chord length: 0.1423 meter (0.4668 ft) Leading-edge radius: 0.0009 meter (0.0031 ft)		Span station: 0.0572 meter (0.1875 ft) Chord length: 0.1267 meter (0.4158 ft) Leading-edge radius: 0.0007 meter (0.0023 ft)		Span station: 0.1880 meter (0.6167 ft) Chord length: 0.0556 meter (0.1823 ft) Leading-edge radius: 0.0003 meter (0.0010 ft)	

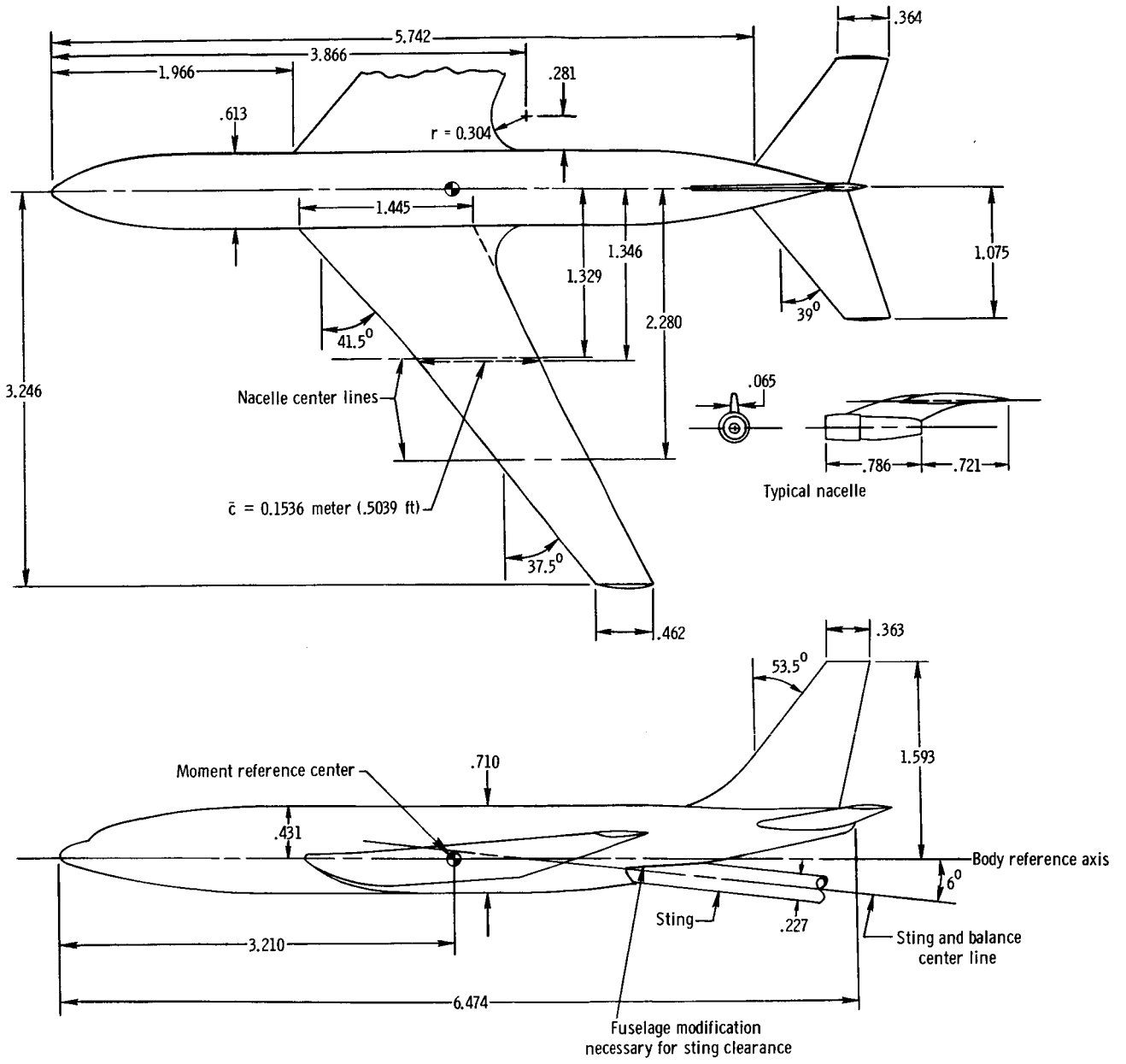

Figure 1.- Geometric details of the model. (Linear dimensions have been nondimensionalized with respect to mean aerodynamic chord.)

L-64-7920.1

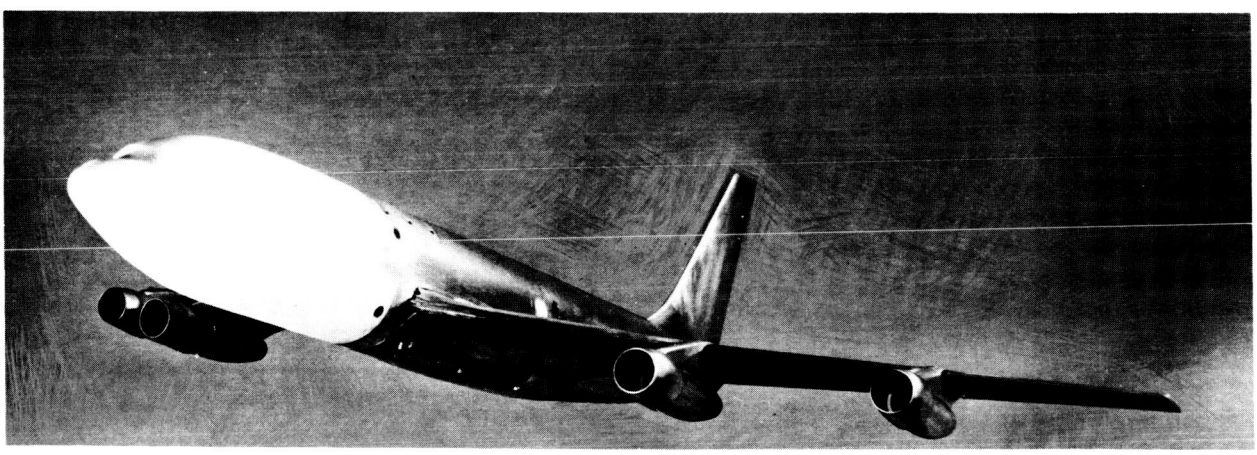

Figure 2.- Photographs of test model.

L-64-7930.1

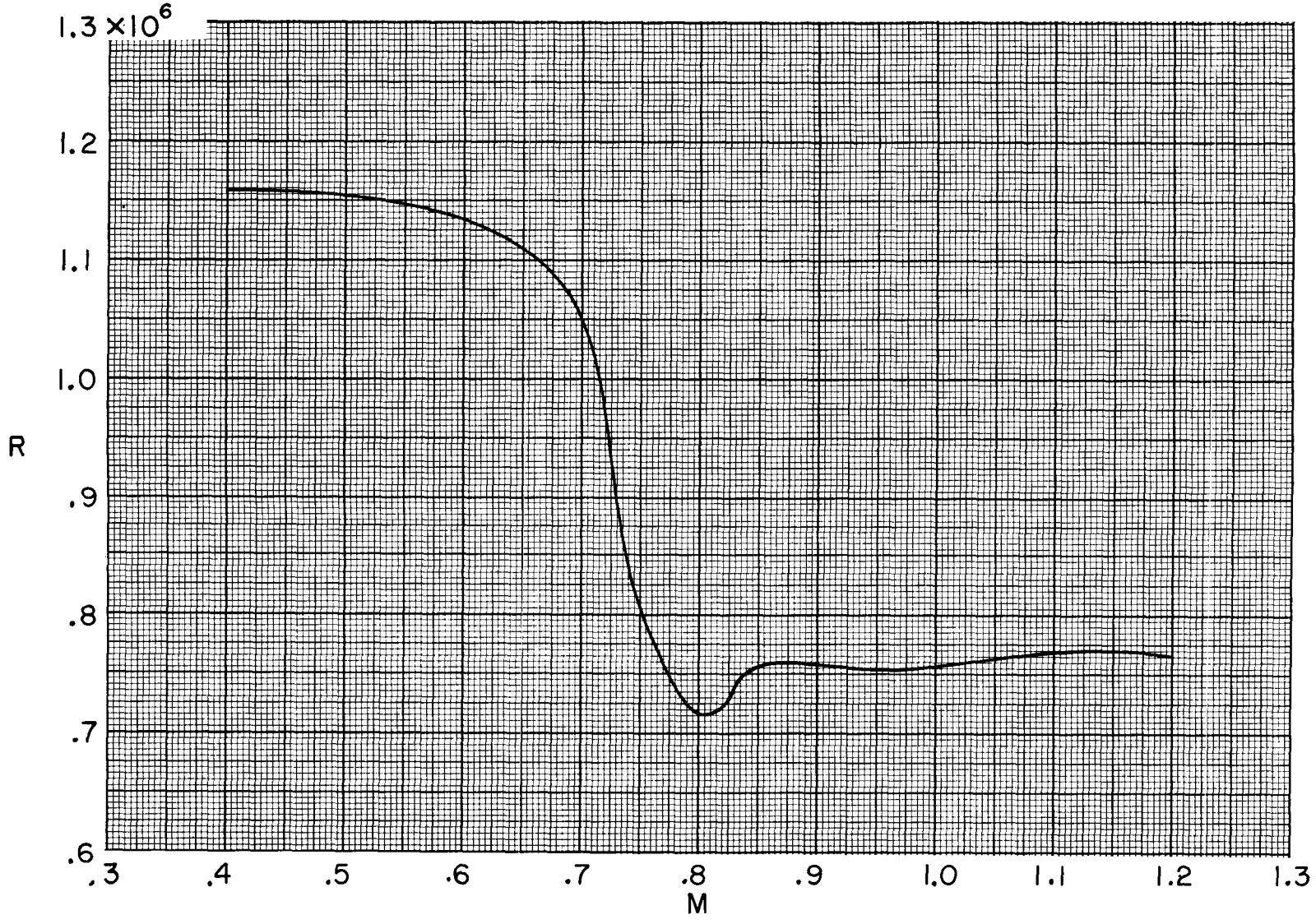

Figure 3.- Variation with Mach number of test Reynolds number based on mean aerodynamic chord.

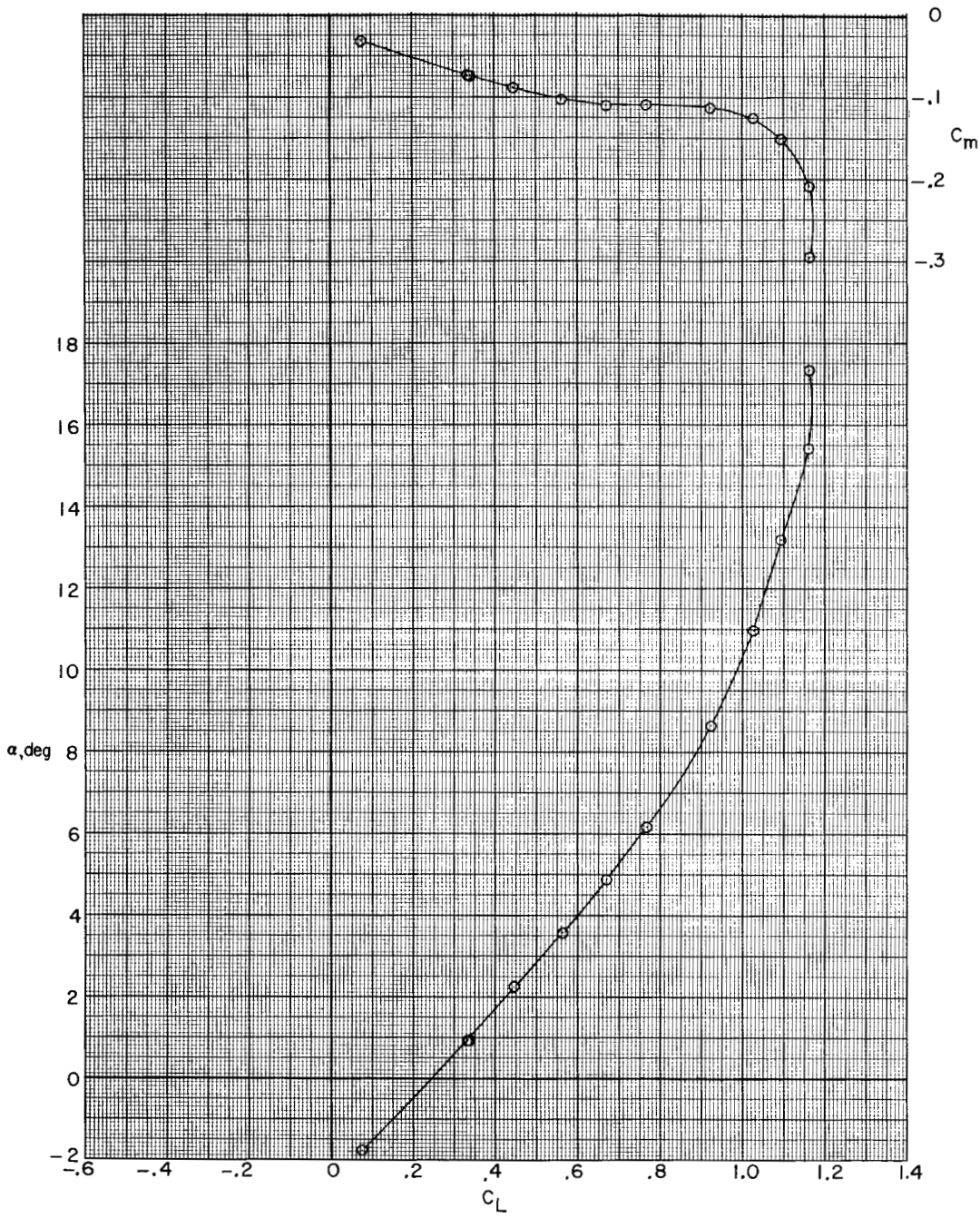

(a) M = 0.40.

Figure 4.- Aerodynamic characteristics in pitch. $\beta = 0^0$.

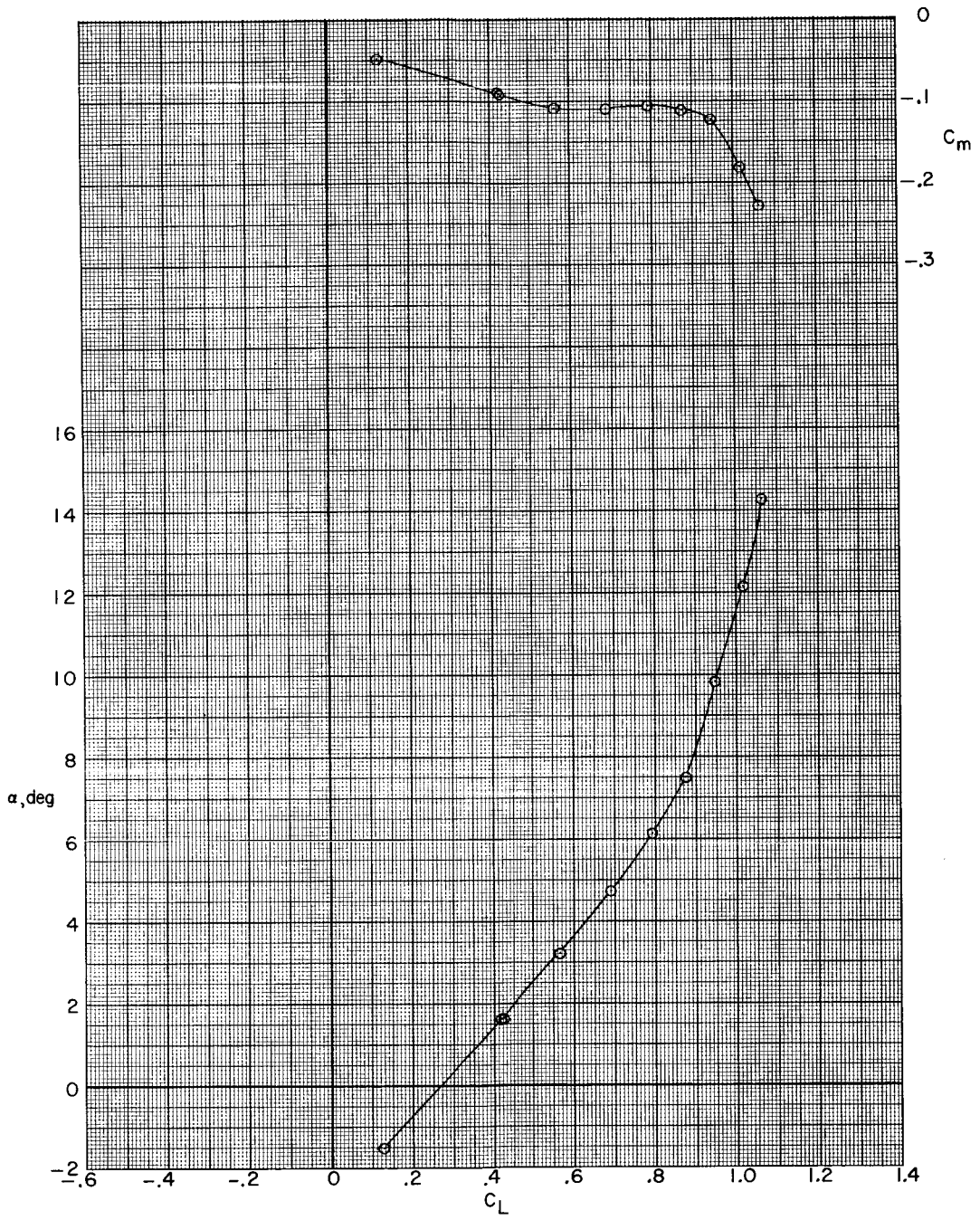

(b) M = 0.60.

Figure 4.- Continued.

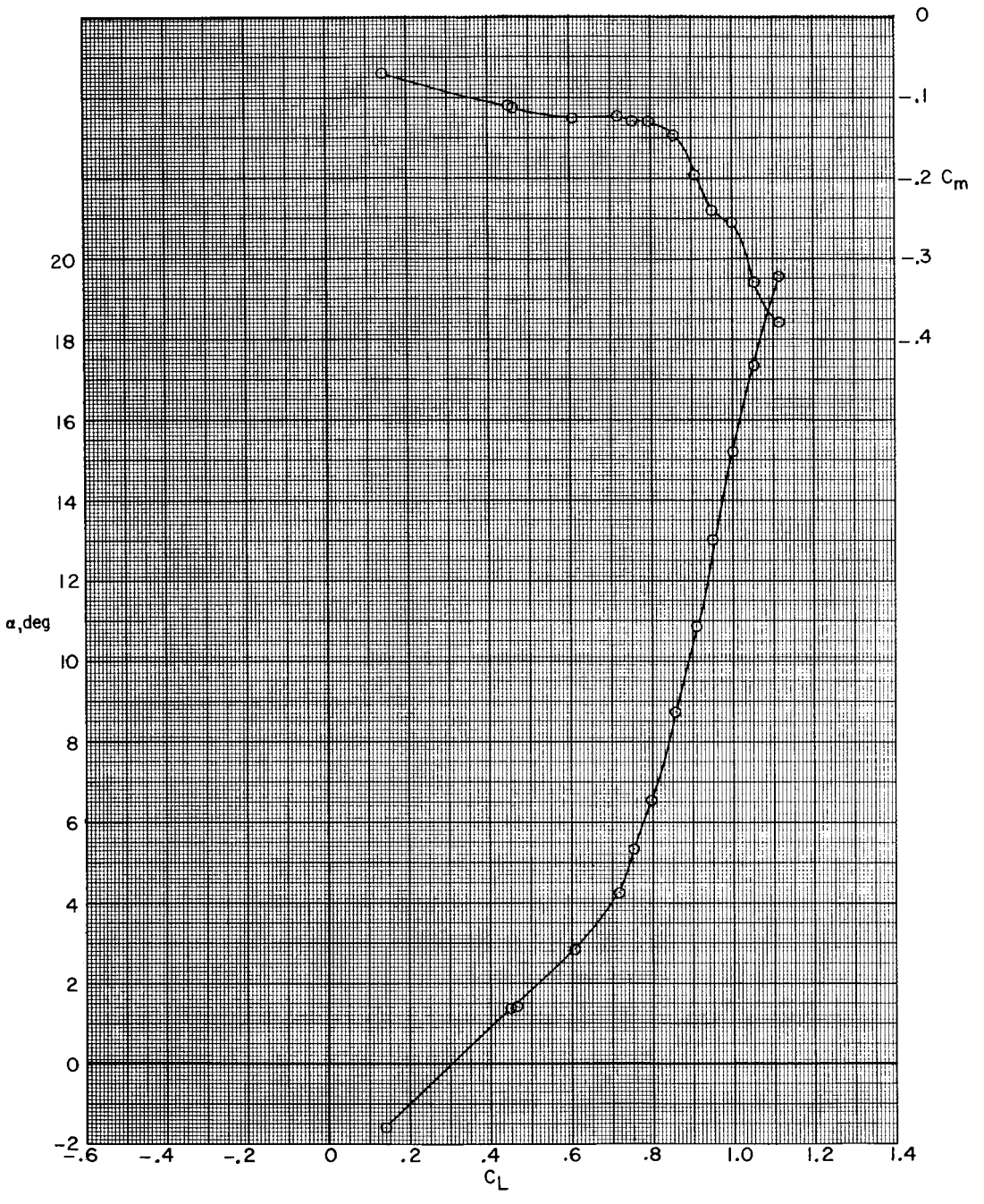

(c) M = 0.80.

Figure 4.- Continued.

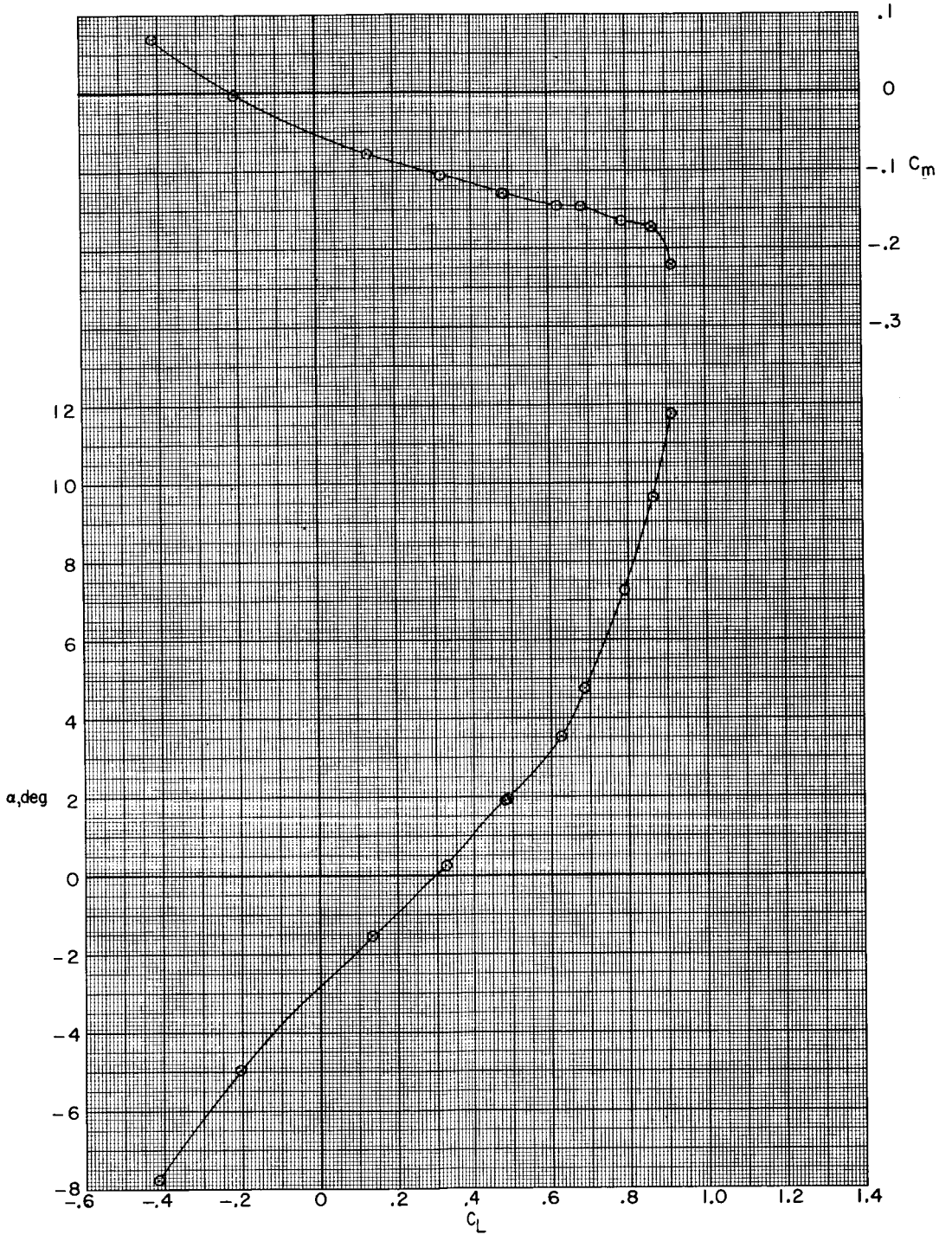

(d) M = 0.85.

Figure 4.- Continued.

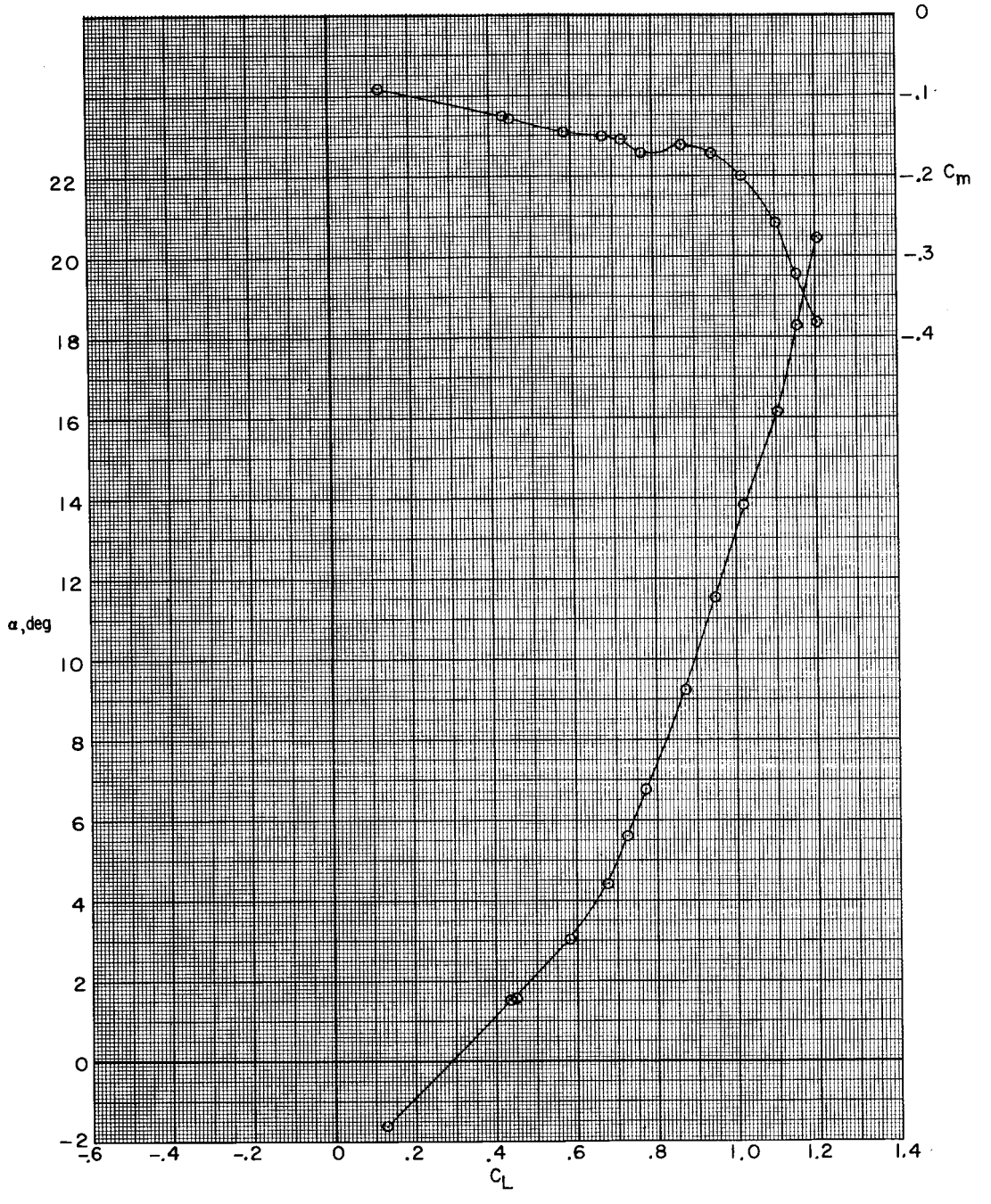

(e) M = 0.90.

Figure 4.- Continued.

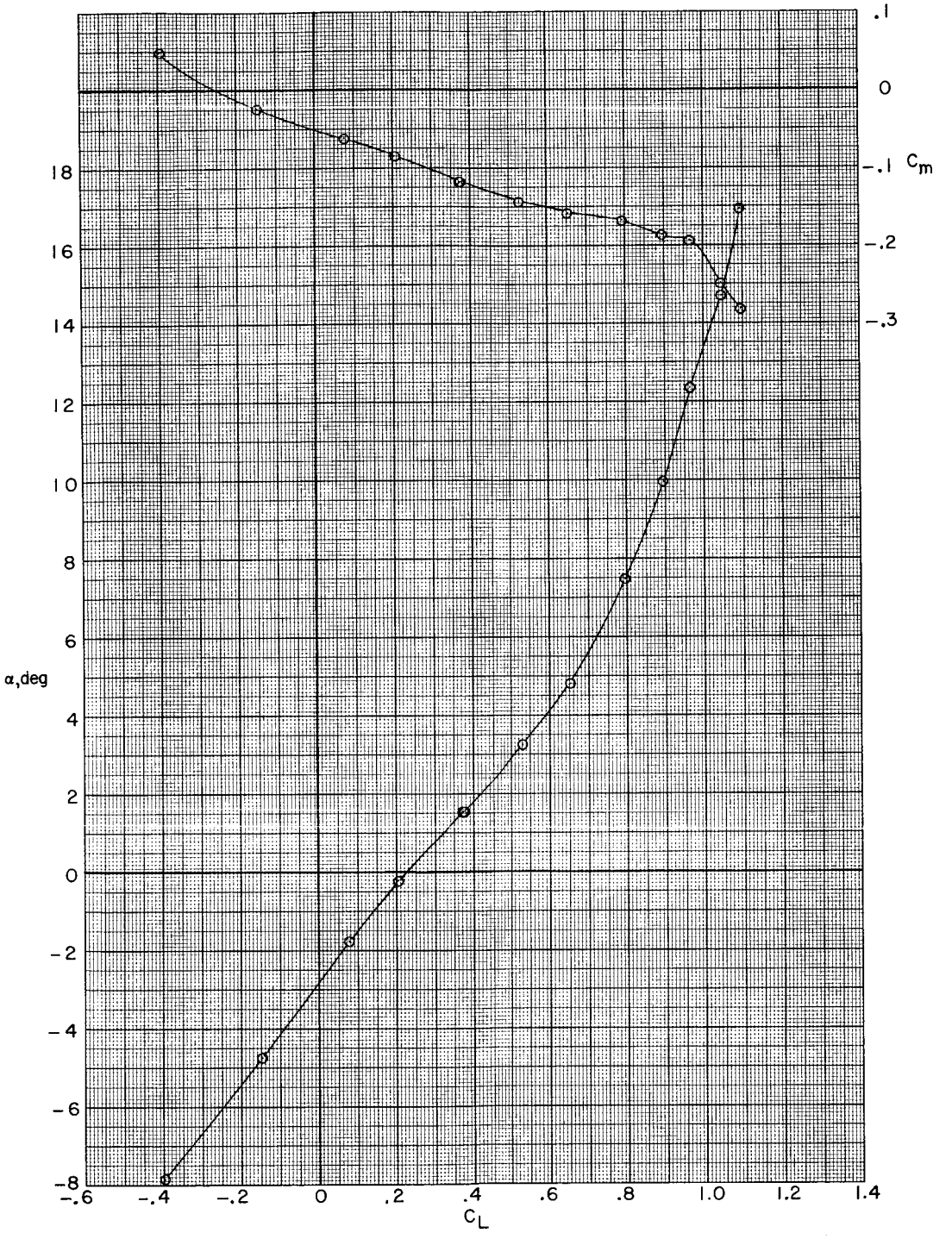

(f) M = 0.925.

Figure 4.- Continued.

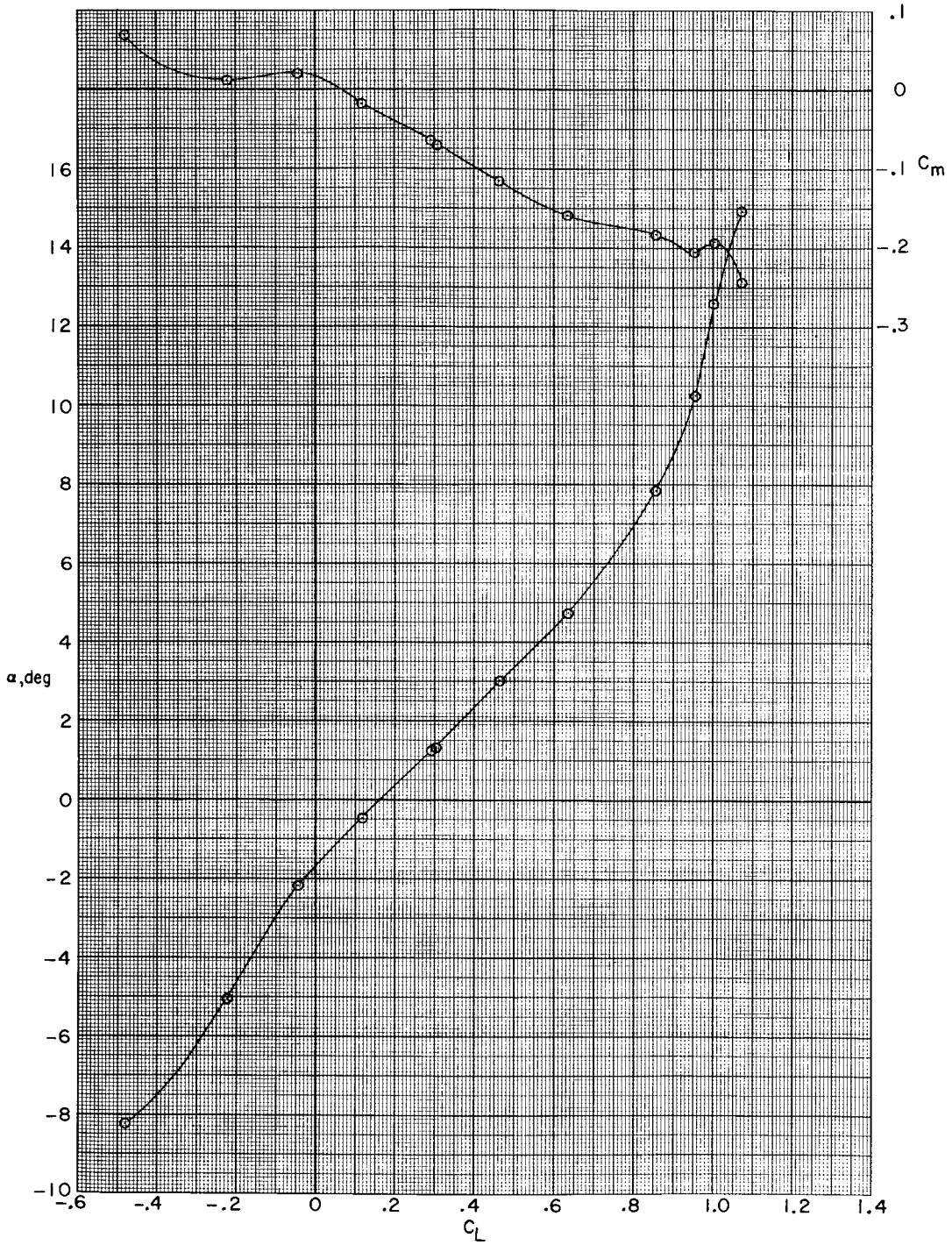

(g) M = 0.95.

Figure 4.- Continued.

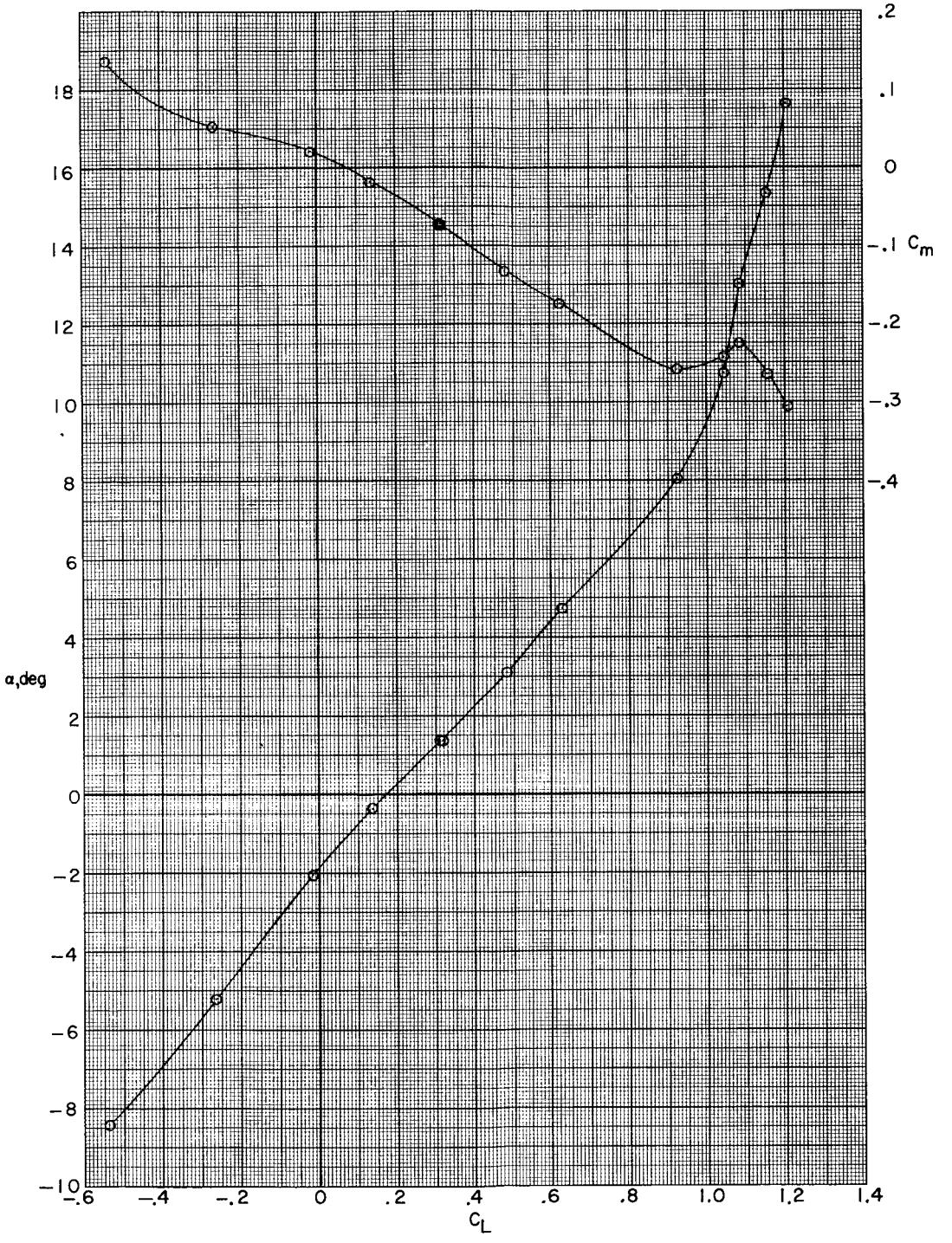

(h) M = 0.975.

Figure 4.- Continued.

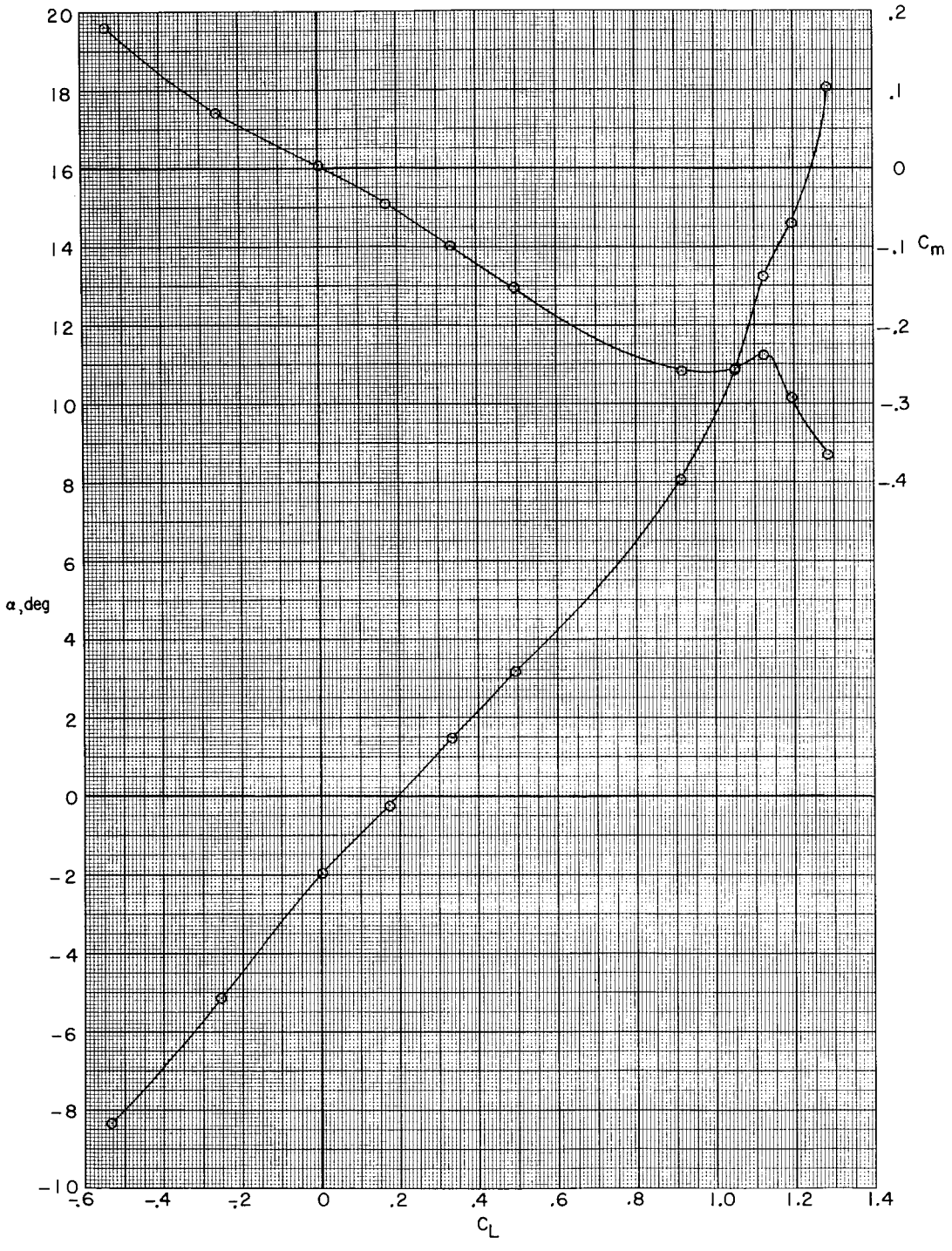

(i) M = 1.00.

Figure 4.- Continued.

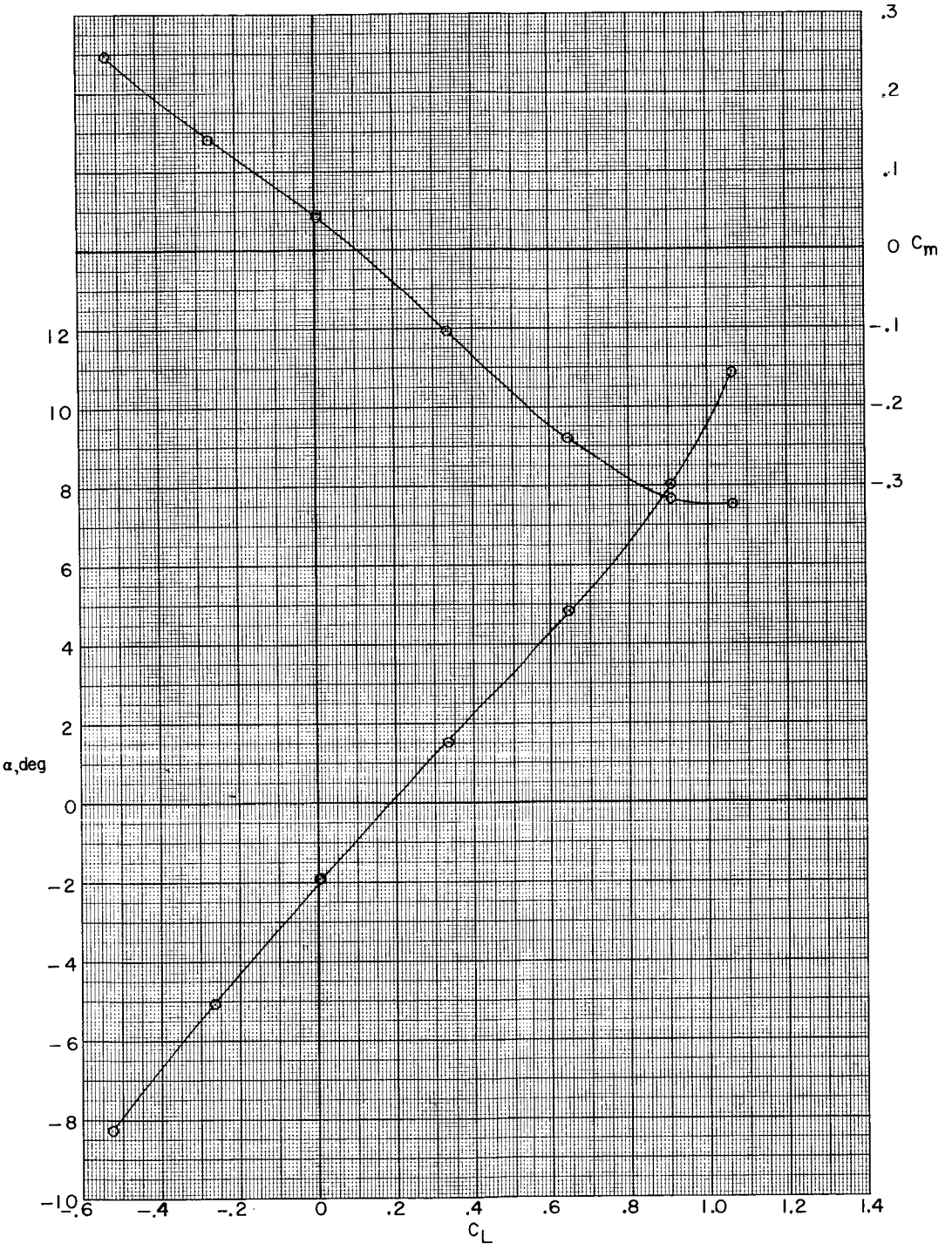

(j) M = 1.03.

Figure 4.- Continued.

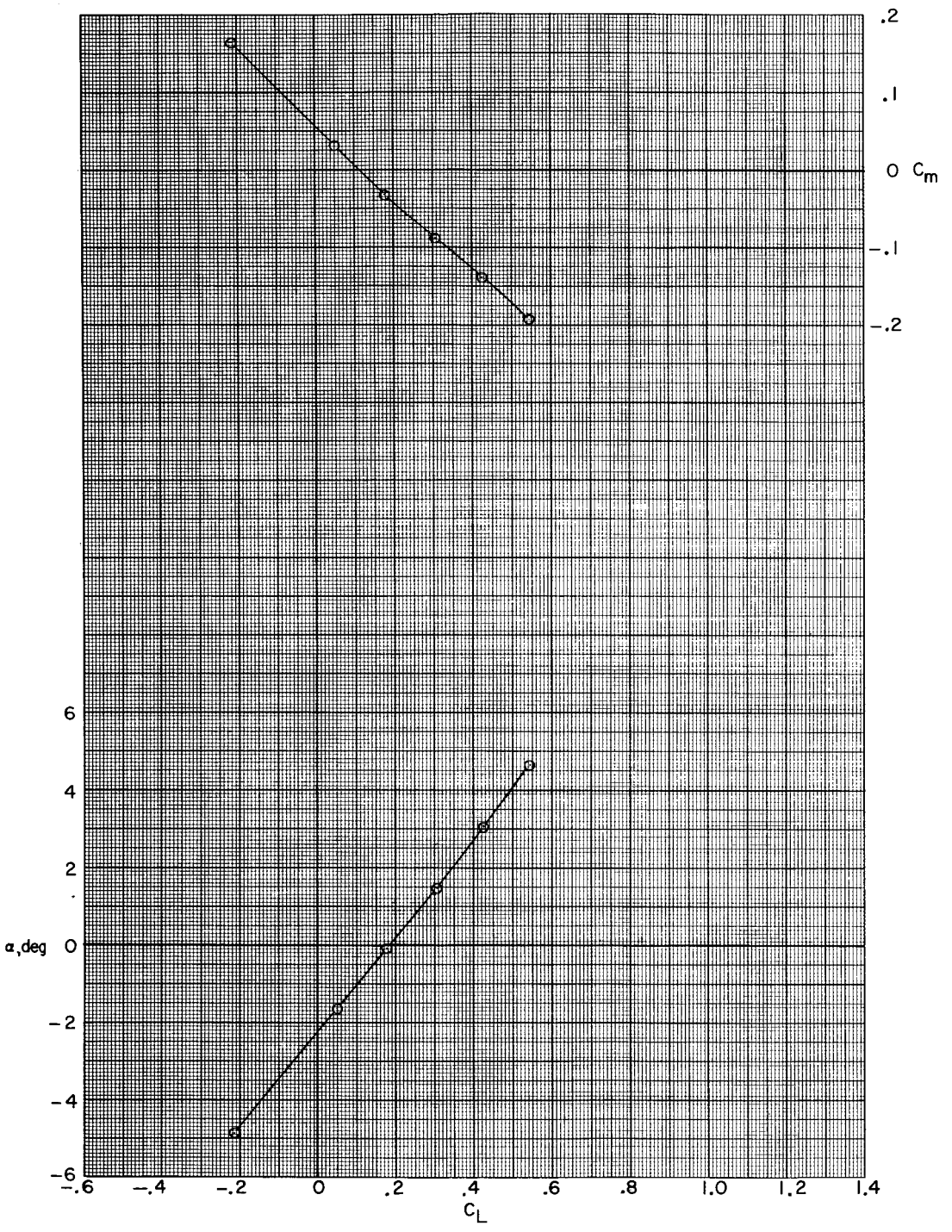

(k) M = 1.20.

Figure 4.- Concluded.

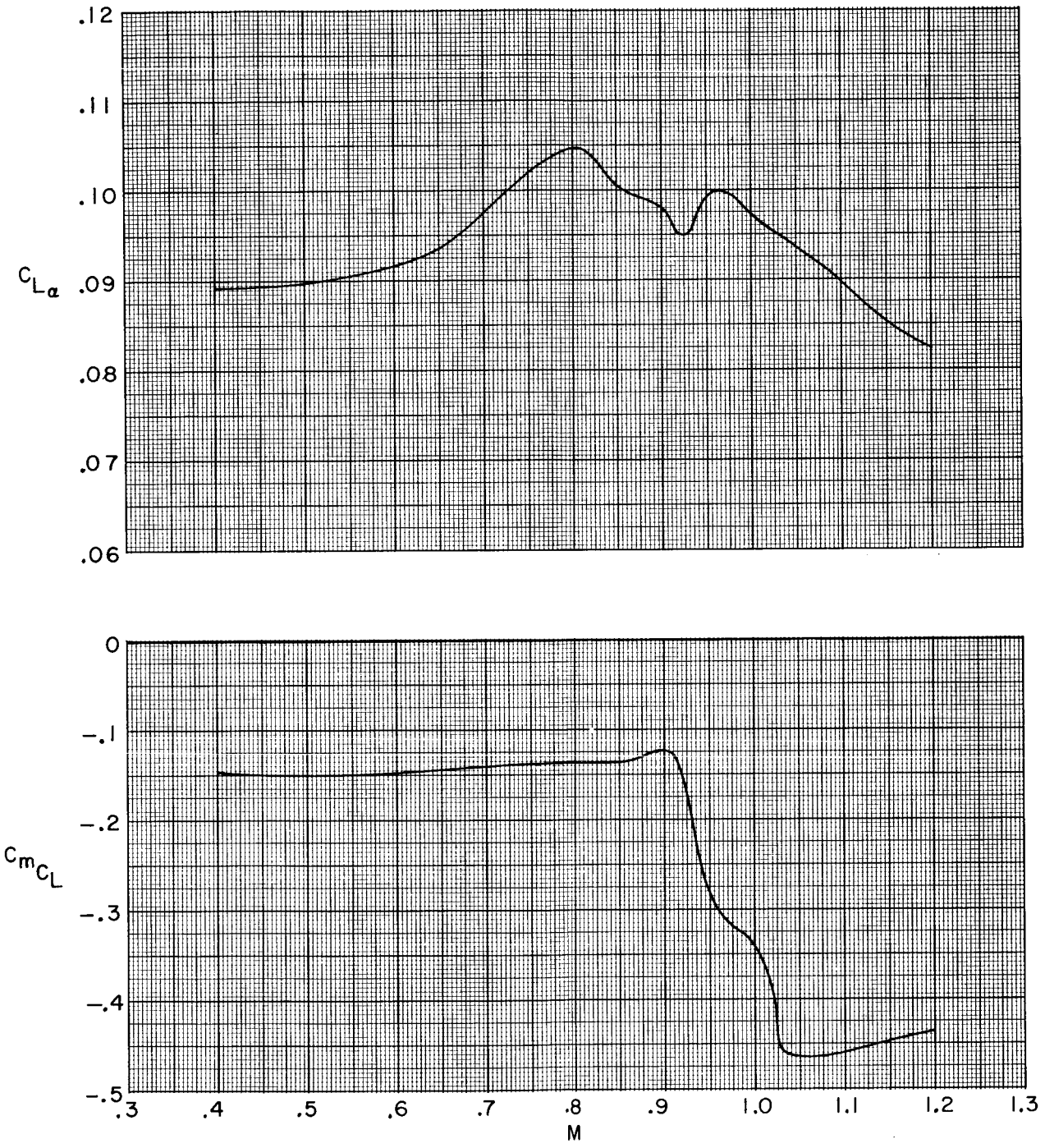

Figure 5.- Variation of lift-curve slope and static longitudinal-stability parameter with Mach number. $\beta = 0^0$.

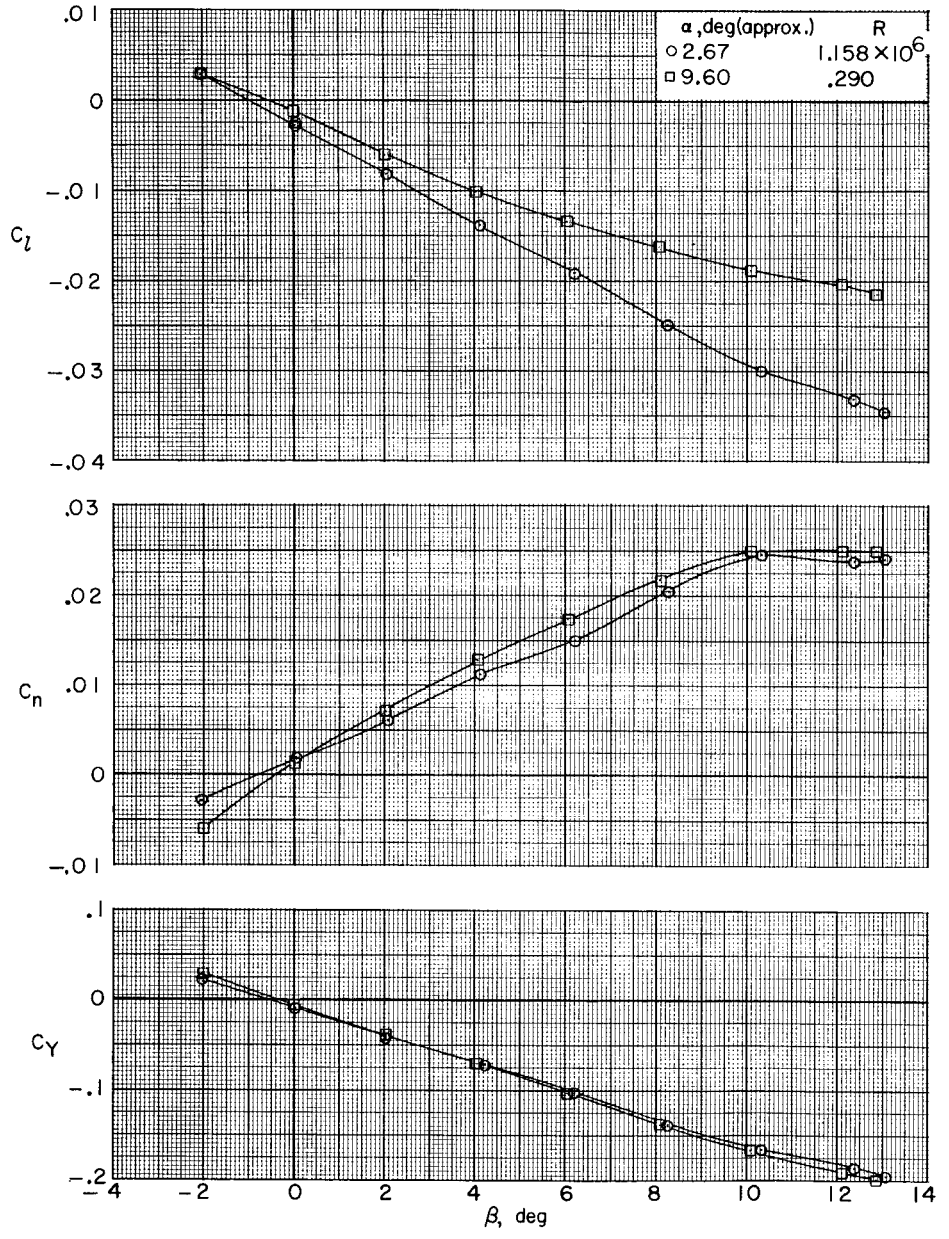

(a) M = 0.40.

Figure 6.- Variation of lateral-stability characteristics with sideslip angle.

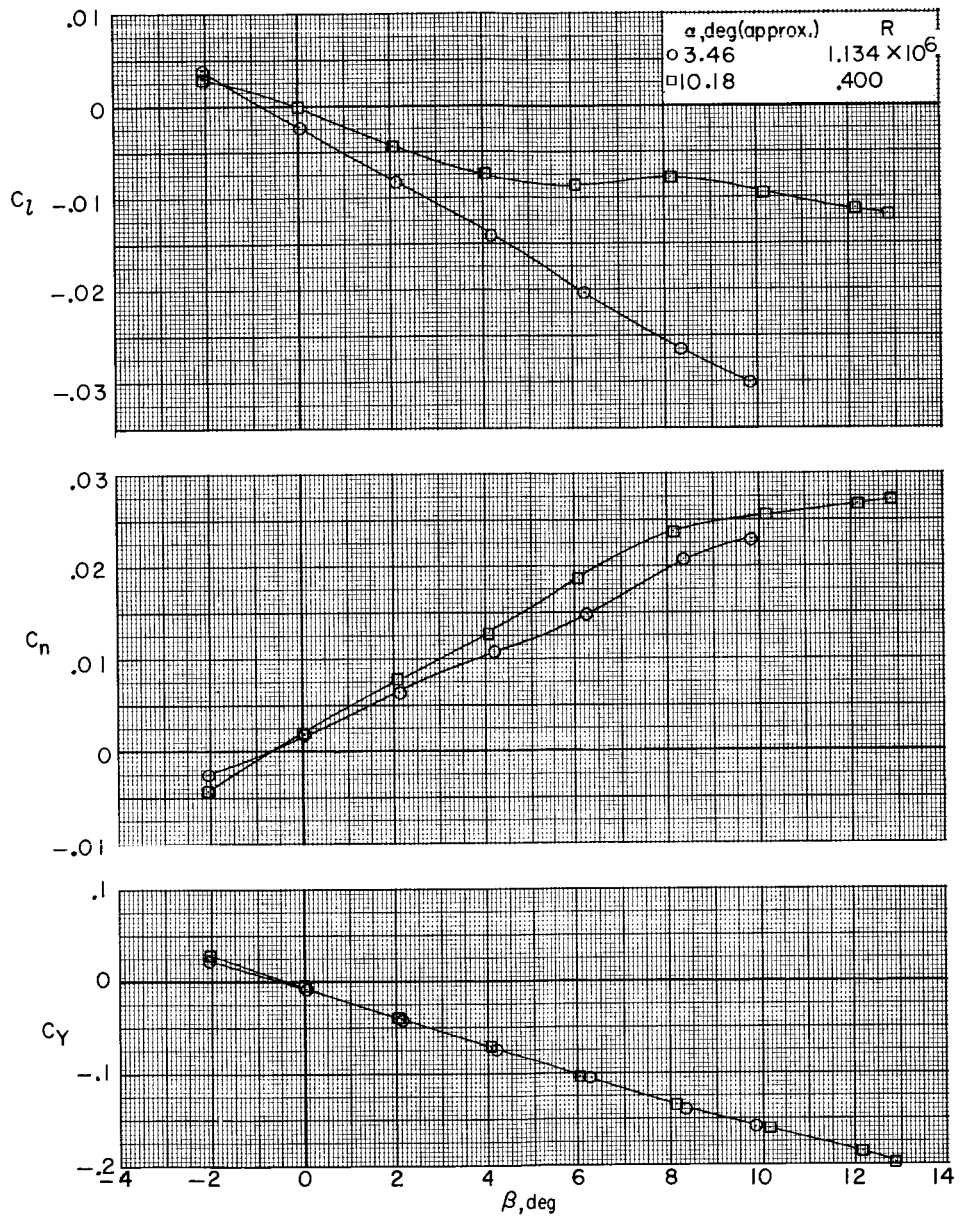

(b) M = 0.60.

Figure 6.- Continued.

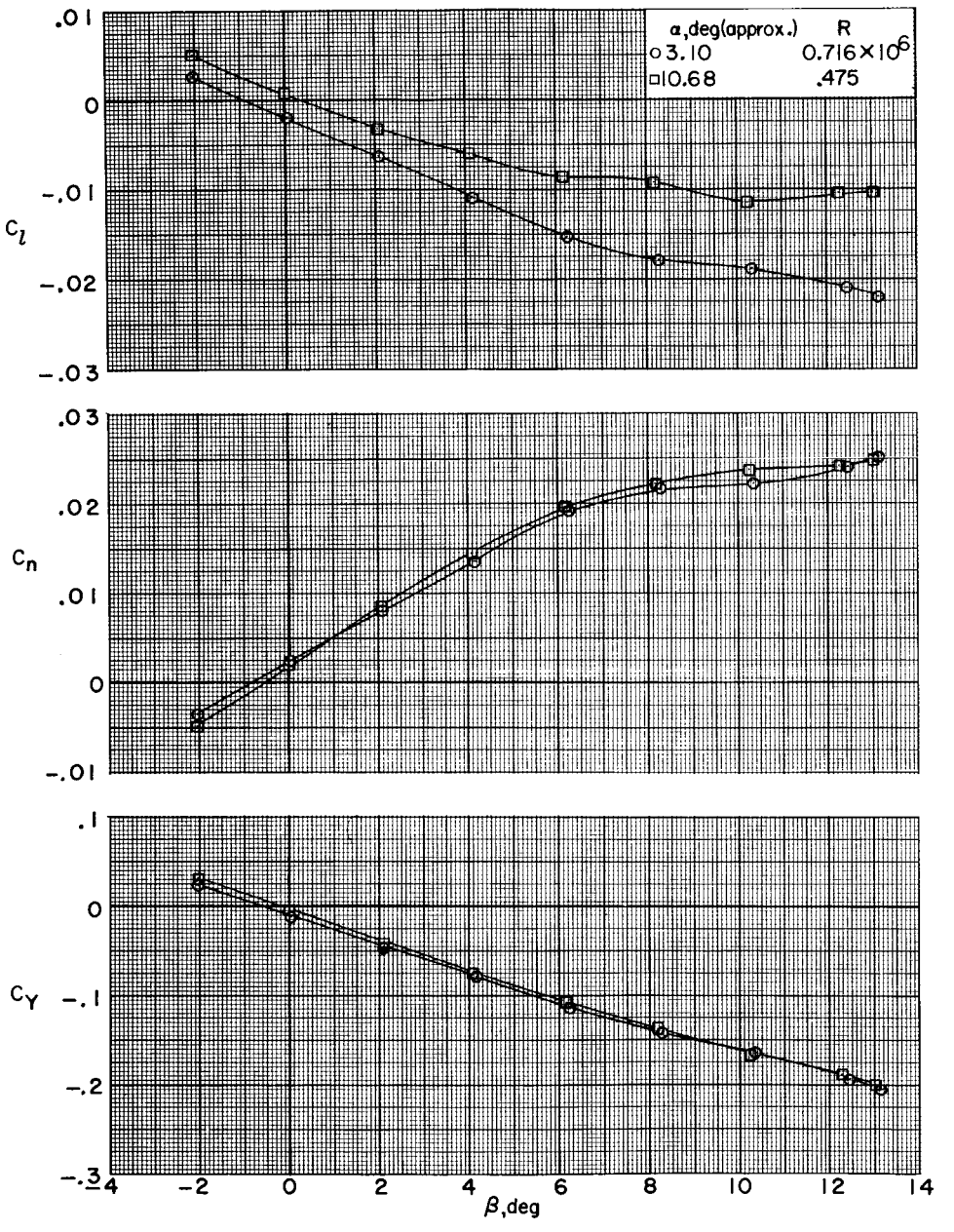

(c) M = 0.80.

Figure 6.- Continued.

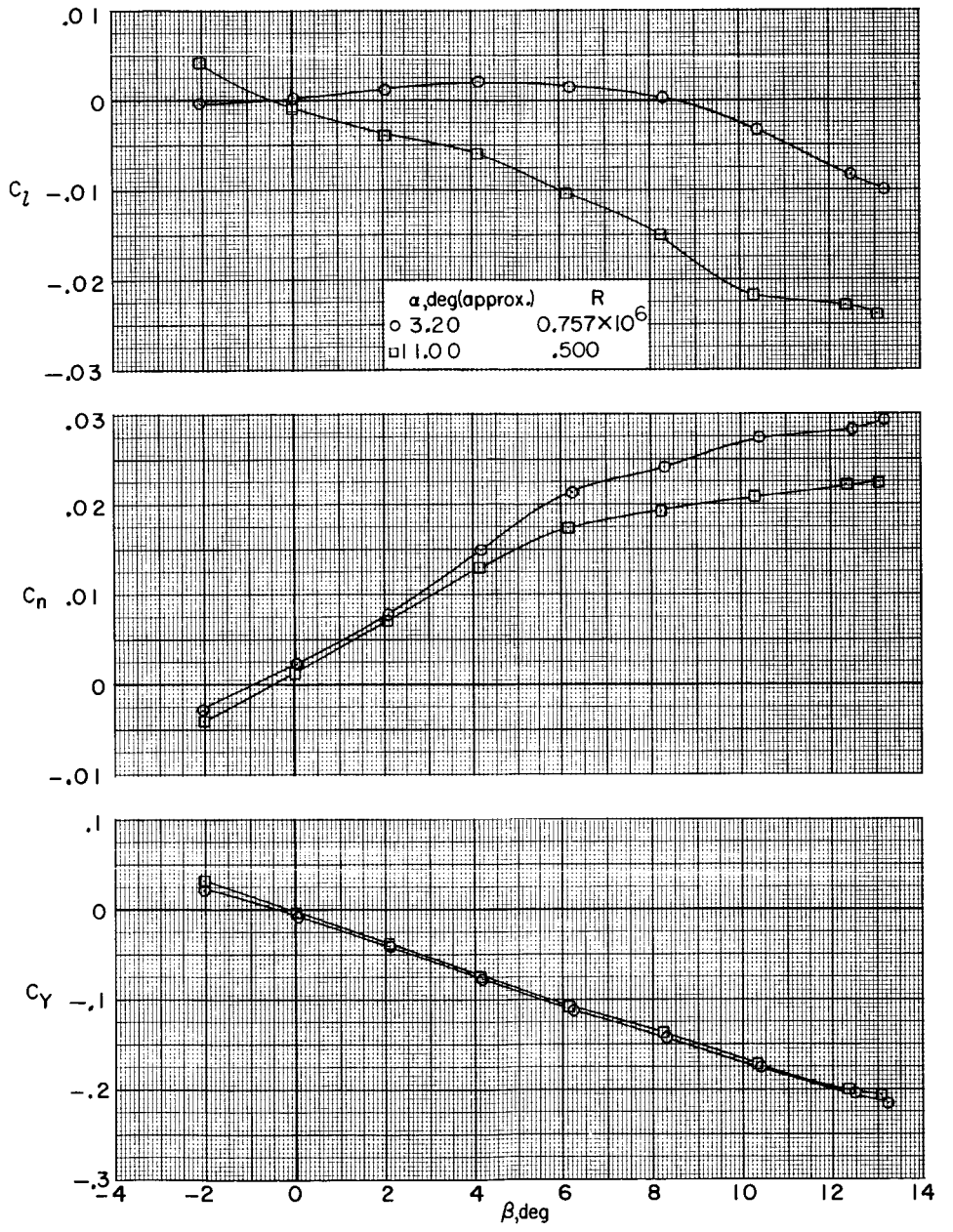

(d) M = 0.90.

Figure 6.- Continued.

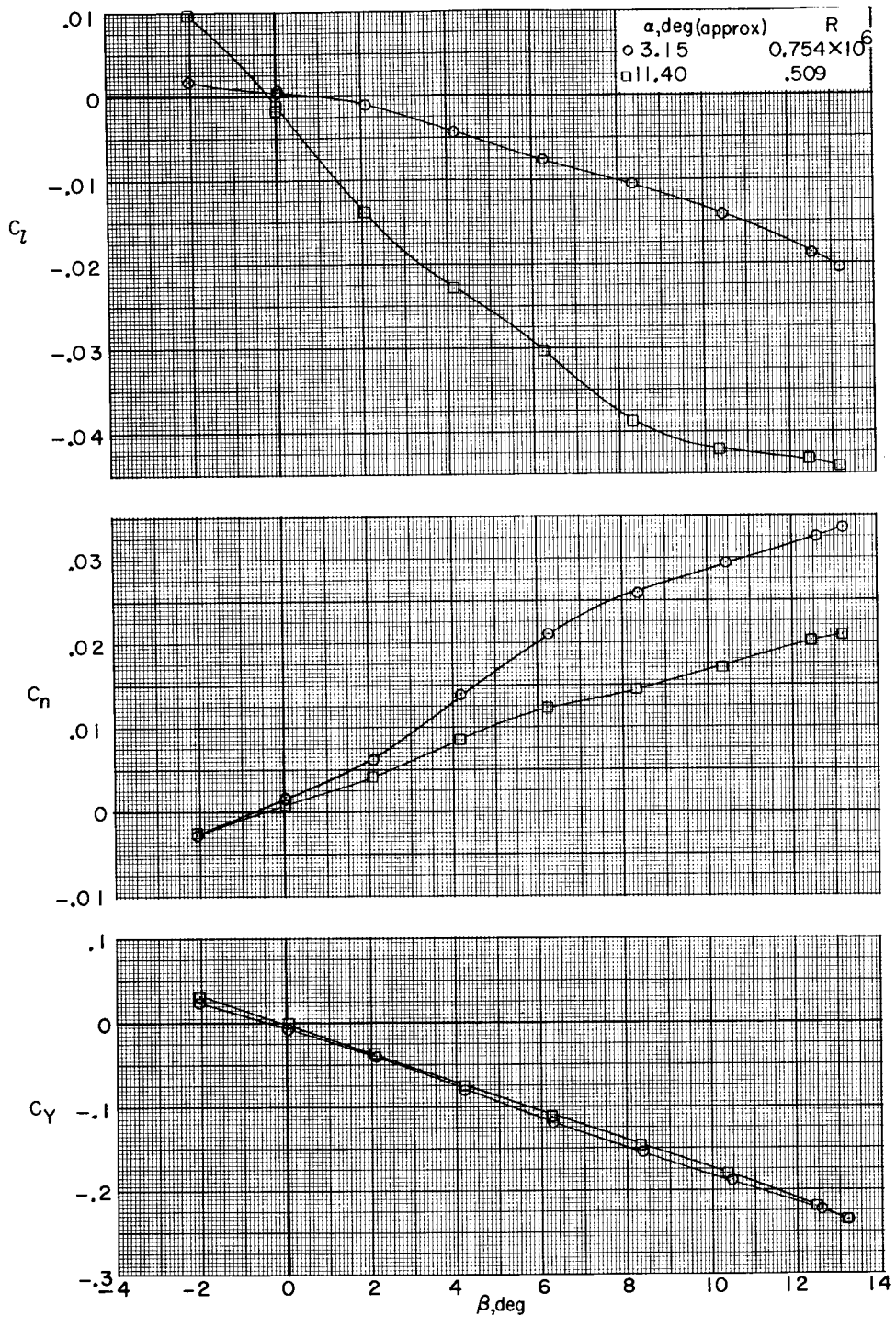

(e) M = 0.95.

Figure 6.- Concluded.

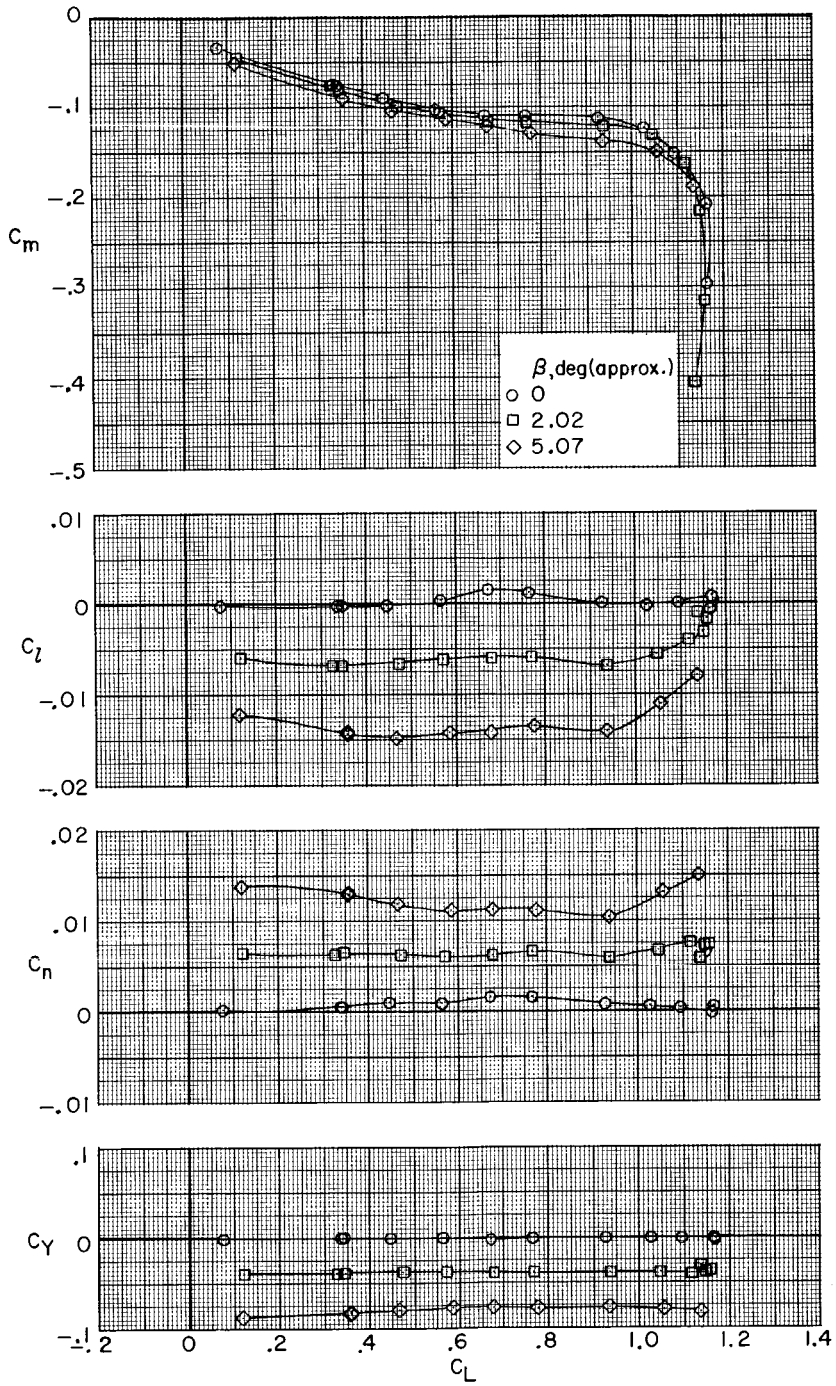

(a) M = 0.40.

Figure 7.- Variation of pitching-moment and lateral-stability characteristics with lift coefficient.

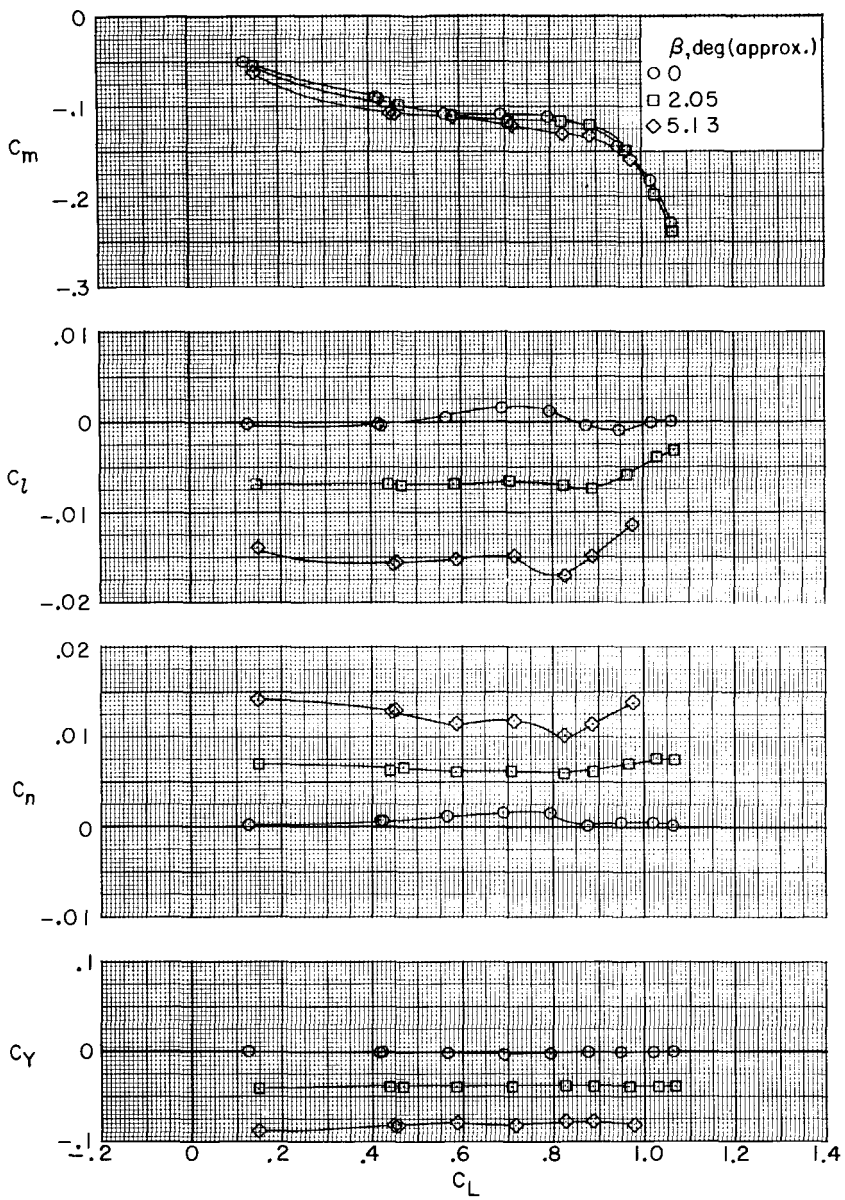

(b) M = 0.60.

Figure 7.- Continued.

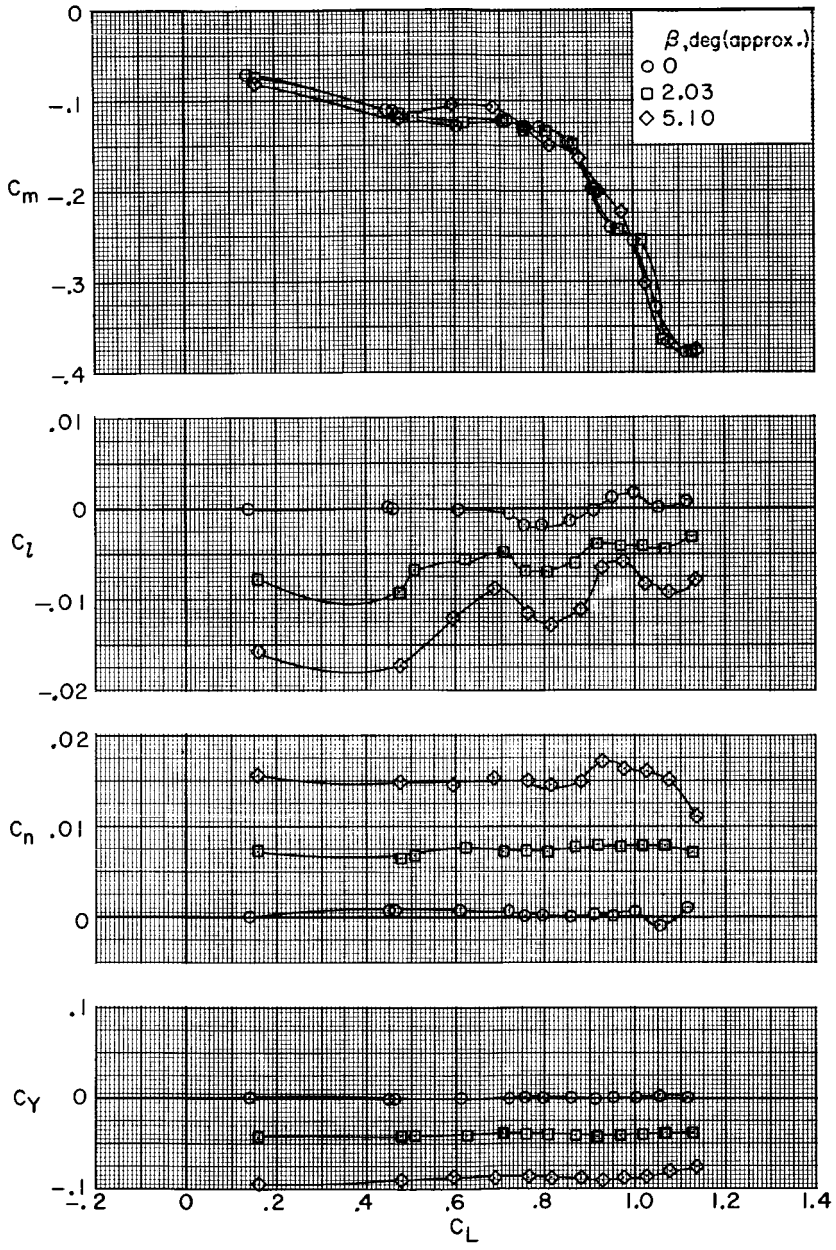

(c) M = 0.80.

Figure 7.- Continued.

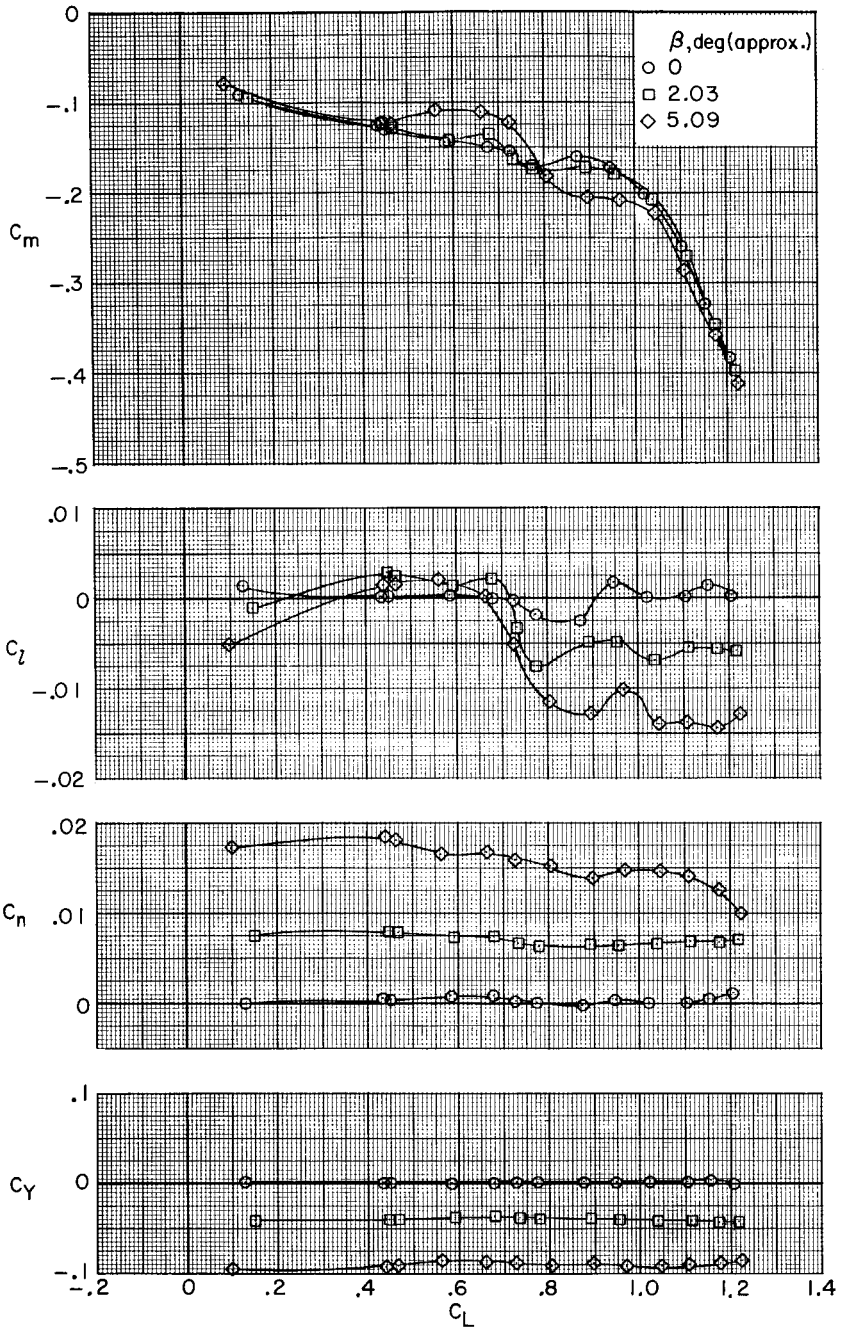

(d) M = 0.90.

Figure 7.- Continued.

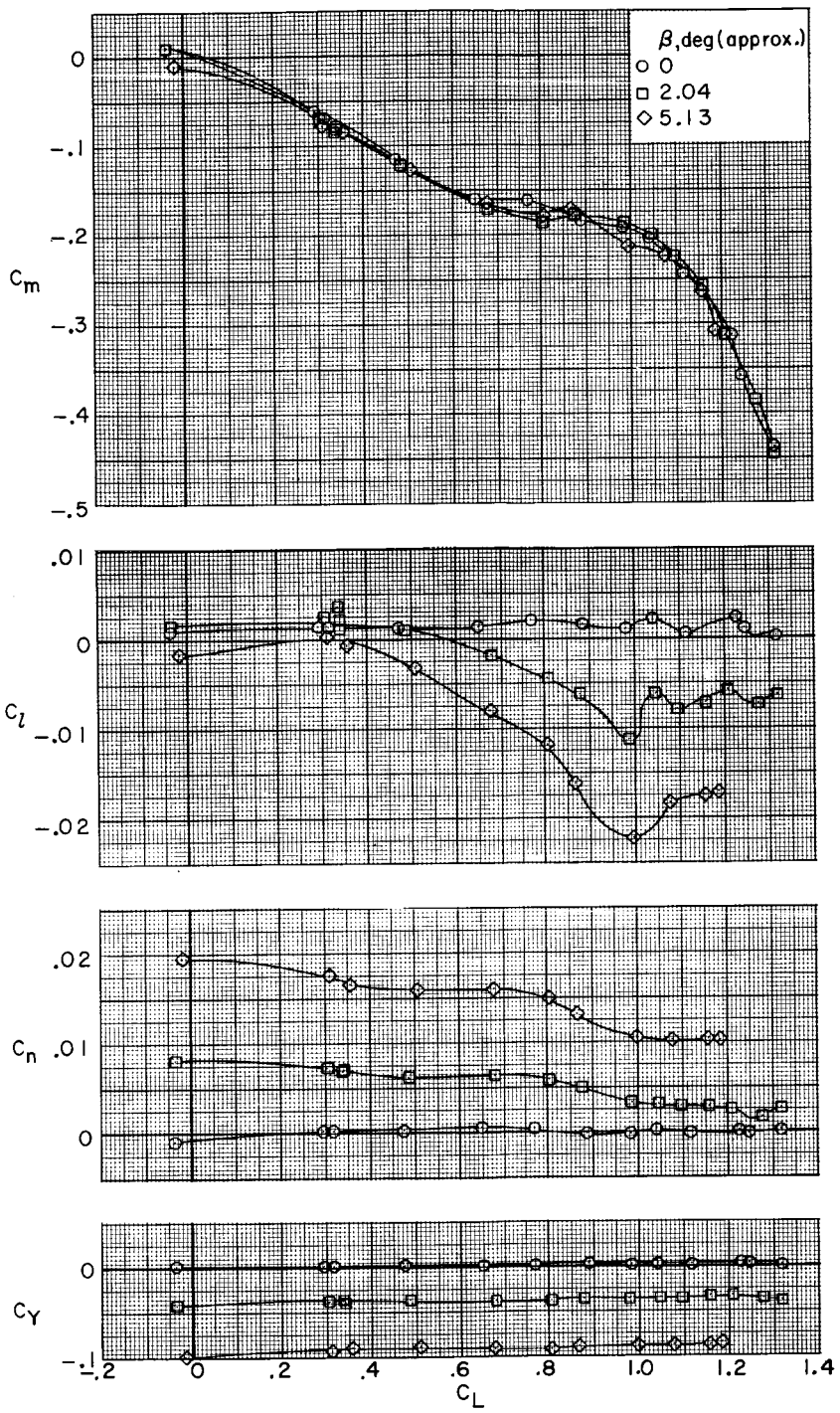

(e) M = 0.95.

Figure 7.- Concluded.

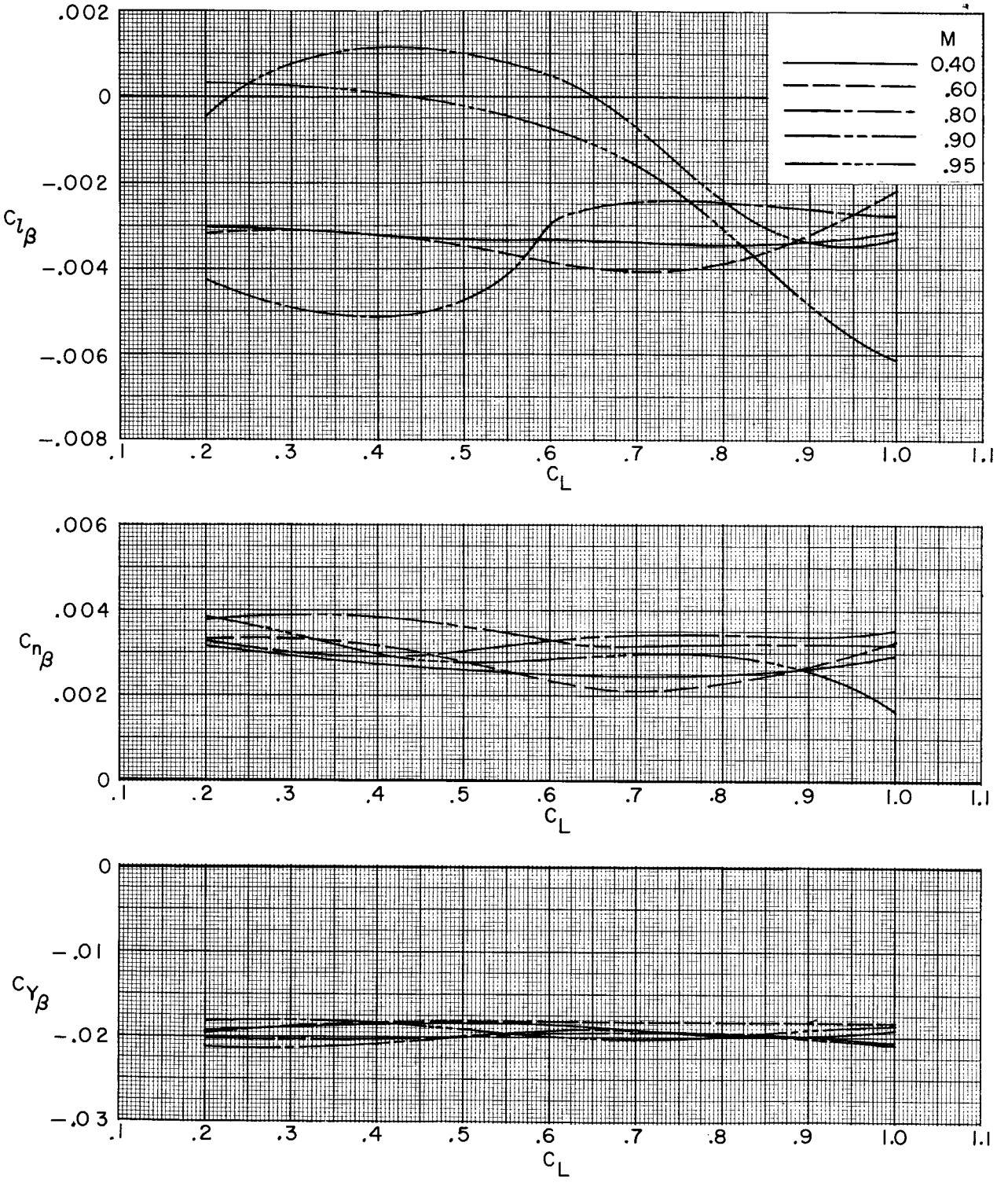

Figure 8.- Variation of lateral-stability derivatives with lift coefficient.

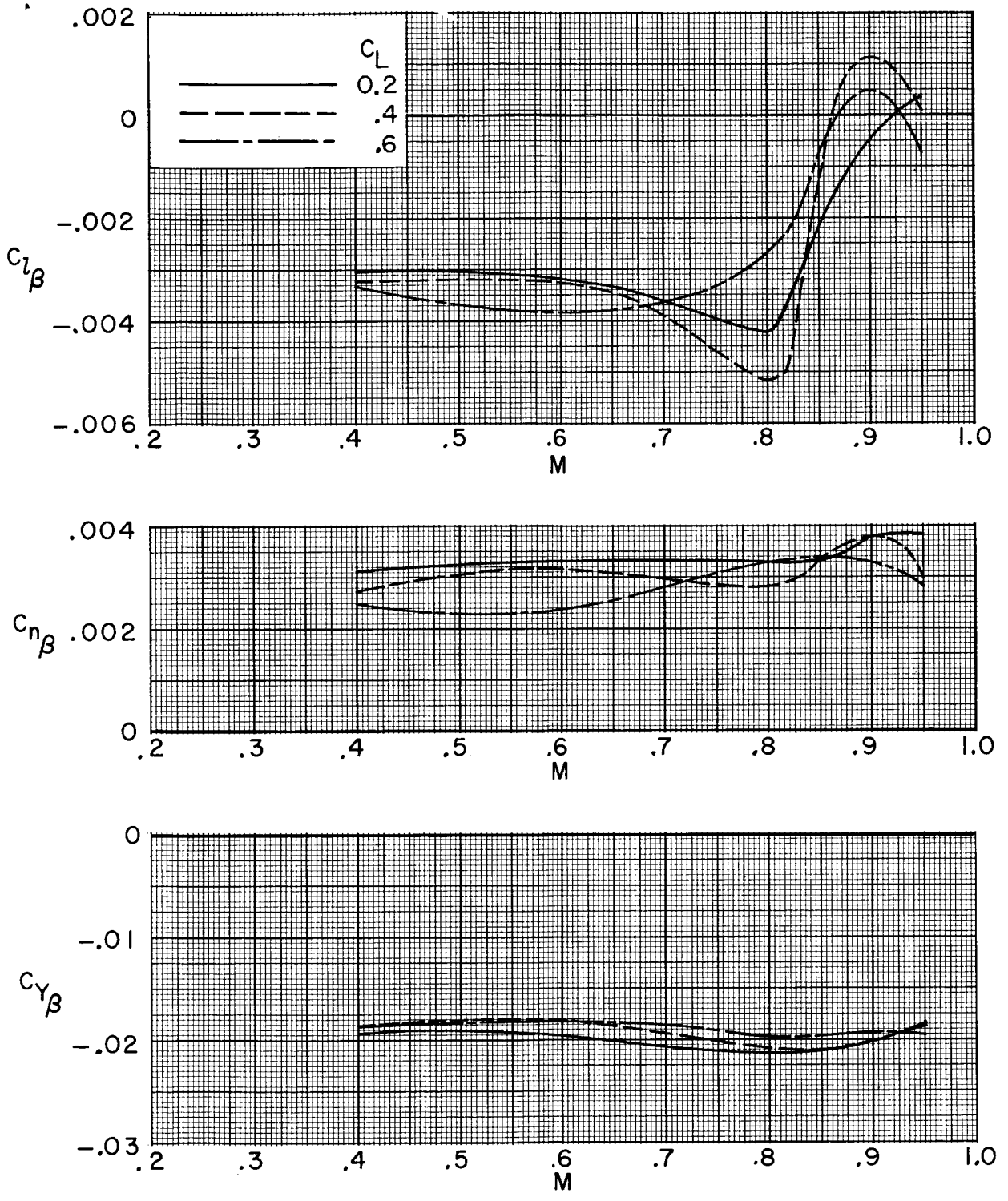

Figure 9.- Variation of lateral-stability derivatives with Mach number.